04/12/2023

Tectono-Stratigraphic Evolution of Salt-Influenced Normal Fault Systems: An Example From The Coffee-Soil Fault, Danish North Sea

Oliver B. Duffy[1*], Rob L. Gawthorpe[2], Matthew Docherty[3]

[1] *Department of Earth and Environmental Sciences, University of Manchester, Manchester, UK, M13 9PL*
[2] *Department of Earth Science, University of Bergen, Allégaten 41, N-5007, Bergen, Norway*
[3] *Exploration Department, Maersk Oil, Esplanade 50, 1263 Copenhagen, Denmark*
**Present Address of Corresponding Author: Bureau of Economic Geology, Jackson School of Geosciences, The University of Texas at Austin, University Station, Box X, Austin, Texas, 78713-8924, USA (e-mail: oliver.duffy@beg.utexas.edu)*

Keywords: North Sea; normal faults; salt tectonics; 3D seismic; fault linkage; fault-related folding; salt-influenced rifting; Danish Central Graben

Abstract

We explore how relationships between fault activity, salt movement, and sediment loading impact hanging-wall stratal geometry throughout the evolution of a salt-influenced normal fault system. We examine a ~65 km long portion of the Coffee-Soil Fault System (CSFS) in the Danish North Sea, the hanging-wall of which has been partially influenced by a pre-rift unit of mobile salt. To constrain the tectono-stratigraphic evolution of the CSFS we combine structural observations with seismic-stratigraphic analysis of hanging-wall growth strata.

We find that the hanging-wall of the CSFS shows major depocentre shifts through time, along with marked variability in along- and across-strike stratal geometries. We explain how the development of these characteristics is influenced by: i) the segmentation and linkage history of the fault system; ii) the evolution of salt-cored cover monoclines above blind basement fault segments; and iii) changes in the locations and rates of accommodation generated by load-driven withdrawal of salt up the hanging-wall dip-slope, and fault-related subsidence. Our findings have

implications for structural and stratigraphic studies in salt-influenced rift basins, as well as for understanding the potential distribution of geo-storage and hydrocarbon reservoirs in such settings.

1. Introduction

Basin-bounding fault systems develop from the propagation, interaction and linkage of initially isolated normal fault segments, attaining final lengths of over 100 km (e.g. Peacock and Sanderson, 1991; Anders and Schlische, 1994; Gawthorpe and Leeder, 2000; McLeod et al., 2000; Nixon et al., 2016). Initially, isolated fault segments are bounded along-strike by regions of low displacement which are expressed locally in the hanging-wall as fault-perpendicular anticlinal highs, whereas regions of high displacement located at segment centres are associated with fault-perpendicular hanging-wall synclinal sub-basin depocentres (*Fig. 1a*) (e.g. Anders and Schlische, 1994; Schlische, 1995; Janecke, 1998; Gawthorpe and Leeder, 2000; Serck and Braathen, 2019). As the isolated fault segments propagate, interact and link, the relief of the fault-perpendicular anticlines decreases and the depocentres coalesce as the loci of hanging-wall subsidence adjusts to the length of the newly-amalgamated fault (*Figs. 1a and b*) (e.g. Anders and Schlische, 1994; Morley, 1999; Cowie et al, 2000; McLeod et al., 2000; Young et al., 2001; Su et al., 2011; Nixon et al., 2016). As such, stratigraphy associated with the earlier fault configuration is preserved at depth and hanging-wall stratal geometries can be used to constrain the growth and linkage histories of normal fault systems (*Fig 1b*) (e.g. Anders and Schlische, 1994; Morley, 1999; Cowie et al, 2000; McLeod et al., 2000; Young et al., 2001; Su et al., 2011; Nixon et al., 2016).

However, the presence of mobile salt may complicate the tectono-stratigraphic evolution of basin-bounding fault systems and thus extra considerations are required when using hanging-wall stratal geometries to constrain growth and segmentation histories in salt-influenced settings (e.g. Nalpas and Brun, 1993; Stewart et al., 1996; 1997; Withjack and Calloway, 2000; Richardson et al., 2005; Soto et al., 2007; Kane et al., 2010; Jackson and Rotevatn, 2013; Lewis et al., 2013; Wilson et al., 2013; Wilson et al., 2023). Richardson et al. (2005) present an example from the Revfallet Fault, Halten Terrace, Offshore Mid-Norway where the upward propagation of faults is impeded by salt, initially restricting them to the sub-salt basement (*Figures 1c and d*). In their ‘pure basement fault’ model, during the early stages of rifting, salt migrates towards the immediate hanging-wall displacement maxima of individual basement faults, passively infilling space created by flexure of the overlying cover (*Fig. 1c*). The salt swells amplify the cover flexure above the blind basement faults, and a syn-rift depocentre develops that is offset into the hanging-wall and that thins onto the swell and towards the fault (*Fig. 1c*). As the basement faults propagate and link along-strike to form a single structure, the salt migrates and coalesces into a single evaporite swell adjacent to the new displacement maximum (*Fig. 1c*). The salt swell amplifies a major cover fold and a single depocentre is offset from the fault (*Fig. 1c*). An alternative scenario is suggested by Kane et al. (2010), using evidence from the Sleipner Fault Zone, Sleipner Basin, South Viking Graben (*Fig. 1e*). Here, the early syn-rift structural style is similar to that interpreted from the Revfallet Fault, with an additional component of hanging-wall sediment-loading which drives the along-strike salt migration (*Fig. 1e*). The salt migrates towards fault segment boundaries, amplifying fault-perpendicular anticlines (*Fig. 1e*). In the late stages of rifting, once the basement fault segments hard-link along-strike and breach the cover fold, the fault-perpendicular anticlines subside in the hanging-wall of the newly-linked fault (*Fig. 1f*). These observations demonstrate that relationships between faulting, salt flow, and sediment loading may modify basin physiography, providing controls upon the spatial and temporal evolution of depocentres in the hanging-wall of border fault systems. However, existing models do not capture the full range of likely relationships that may occur along salt-influenced border faults. Thus, key aspects remain to be explored including how interactions between salt flow, sediment loading and faulting are influenced by: i) a lateral variation in salt thickness and mobility along-strike of a bounding fault system; ii) settings marked by pronounced hanging-wall sediment loading.

To address these aspects, we examine the growth and linkage history of a ~65 km long portion of the Coffee-Soil Fault System (CSFS), a basement-rooted border fault system in the Danish North Sea influenced by: i) Late Permian Zechstein salt of variable thickness and mobility; ii) Triassic and Jurassic-Early Cretaceous rifting; and iii) pronounced syn-rift sediment loading in hanging-wall depocentres and associated salt flow (Duffy et al., 2013). We integrate structural data along with analysis of hanging-wall stratigraphy to i) reconstruct the tectono-stratigraphic evolution of the CSFS; and ii) examine how interactions between faulting, sediment loading, and salt flow contribute to the marked variability in hanging-wall stratal geometry observed along strike of the CSFS.

2. Structural and Stratigraphic Framework

The NNW-SSE-trending Danish Central Graben consists of a series of 10-50 km long and 5-30 km wide half-grabens bounded by predominantly west-dipping normal faults which have developed as a consequence of Permo-Triassic and Mid-Jurassic-Early Cretaceous rifting (*Figs. 2-3*) (Ziegler, 1975; Gowers and Sæbøe, 1985; Stemmerik *et al*., 2000; Møller and Rasmussen, 2003). The Tail-End Graben and Salt Dome Province are located in the east of the Danish Central Graben, and are bounded to the east by the CSFS, a west-dipping border fault system which extends for over >>65 km (*Fig. 2*). Previous studies have highlighted segmentation along-strike of the CSFS, with fault segments ranging in length from 5-30 km (Cartwright, 1987; Bruhn and Vagle, 2005). This study focuses on a *ca.* 65 km long portion of the CSFS which consists of three principal components; a NW-SE-striking Northern Fault which is >25 km in length and extends outside of the survey area to the north, and the NNW-SSE- to N-S-striking Southern Faults A and B which have a combined length of >40 km (*Fig. 4*).

During the Late Permian, the salt-rich Zechstein Supergroup was deposited in the southern Tail-End Graben and Salt Dome Province (*Figs. 2 and 3*) (Gowers and Sæbøe, 1985; Taylor, 1998; Møller and Rasmussen, 2003; Tanveer and Korstgård, 2009). The study area straddles the boundary between both the initial and present-day northern pinch-outs of the mobile (halite-rich) component of the Zechstein Supergroup (*Figs. 2 and 4*) (Gowers and Sæbøe, 1985; Duffy et al., 2013). North of this pinchout, in the hanging-wall of the Northern Fault and the majority of the Poul Plateau, Duffy et al. (2013) define a domain characterised by a Zechstein depositional thickness of <100 ms TWT and without a mobile halite component (*see also* Gowers and Sæbøe, 1985). In contrast, south of the pinchout and in the hanging-wall of the Southern Fault, the Zechstein reaches depositional thicknesses of *ca*. 200-500 ms TWT with the presence of salt pillows and diapirs suggesting the salt contains a significant mobile halite component (*Fig. 4;* Duffy et al., 2013). The lateral variability in the thickness and mobility of the Zechstein salt has provided a basin-scale control upon the structural styles and depocentre geometries developed within the overlying rift-influenced Triassic and Jurassic units in both the southern Tail-End Graben and Salt Dome Province (Sundsbø and Megson, 1993; Rank-Friend and Elders, 2004; Duffy et al., 2013) and elsewhere across the Central North Sea (e.g. Hodgson et al., 1992; Erratt et al., 1993; Stewart et al., 1997; Stewart and Clark, 1999; Dooley et al., 2005; Karlo et al., 2014; Ge et al., 2017; Jackson and Stewart, 2017; Jackson et al., 2018).

Previous studies have identified a period of rifting within the Triassic (herein termed ‘Rift Phase 1’) which, in the halite-rich portions of the Danish Central Graben, coincided with a phase of halokinesis resulting in the development of pillows, diapirs and withdrawal-related depocentres (*Fig. 3*) (Cartwright, 1991; Korstgård et al., 1993; Rank-Friend and Elders, 2004; Duffy et al., 2013). Following the collapse of the Early Jurassic Mid-North Sea Dome, a renewed period of fault-controlled subsidence (herein termed ‘Rift Phase 2’) influenced the Danish Central Graben in the Mid-Jurassic to Early Cretaceous (*Fig. 3*) (Ziegler, 1990; Møller and Rasmussen, 2003). This major rift phase is defined seismically as the interval between the base of the Mid-Jurassic succession and the Base Cretaceous Unconformity (*Fig. 3*). Rift Phase 2 occurred in three episodes, with displacement on both N-S-striking and NNW-SSE-striking faults (*Fig. 3*) (Møller and Rasmussen, 2003). Upper Aalenian-Callovian rifting is associated with the deposition of the sand-rich Bryne and Lulu formations, whilst in the Oxfordian to Ryazanian phases of rifting, deepening associated with the rift climax resulted in the deposition of up to 3000 m of offshore to basinal mudstones of the Lola and Farsund formations (*Fig. 3*) (Møller, 1986; Andsbjerg and Dybkjær, 2003; Møller and Rasmussen, 2003). From the Hauterivian through to the Neogene, the Danish Central Graben experienced several phases of inversion, expressed variably across the study area by large-wavelength, low-amplitude inversion anticlines, and reverse reactivation of normal faults (Cartwright, 1989; Vejbæk and Andersen, 2002; Rasmussen, 2009; Hansen et al. 2020).

3. Dataset and Methods

The study area covers 717 km^2 of the Danish Central Graben, focused around the Coffee-Soil Fault System in the southern portion of the Tail-End Graben and the northern part of the Danish Salt Dome Province (*Fig. 2*). The seismic data are time-migrated, zero phase, and of European polarity (positive reflection coefficient is displayed in red), with inlines (E-W) and crosslines (N-S) at a line spacing of 25 m.

Stratal terminations and abrupt changes in seismic facies were used to define nine regionally-mappable seismic horizons across pre-, syn- and post-rift intervals (*Fig. 3;* see methods of Duffy et al., 2013). The horizons also define the overall geometry and throw characteristics of the CSFS at sub- and supra-Zechstein levels, as well as highlight key internal characteristics within the syn-rift sequence. The ages of the seismic horizons were constrained using eleven wells, each containing a standard suite of borehole data, although no wells penetrated below the Triassic (*Figs. 2-3*).

Thickness maps for successive intervals, in combination with the architecture of hanging-wall stratigraphy, were used to determine the spatial and temporal evolution of faults, folds and salt structures (*Fig. 3*).

To ensure that seismic reflection geometries analysed within this study are not overprinted by post-rift inversion, seismic sections which trend parallel to the inferred predominant NNE-SSW inversion stress regime (Cartwright, 1989; Vejbæk and

Andersen, 2002; Hansen et al., 2020) are flattened on a local intra-Cretaceous reflection.

4. Structural Style of the Coffee-Soil Fault System

4.1. Top pre-Zechstein Structural Characteristics

Present-day, the region between the Northern Fault and Southern Fault A is breached by an 8 km long, E-W-trending jog and is associated with a regional basement high known as Poul Plateau (*Figs. 5 and 6*) (Duffy et al., 2013). The configuration of CSFS components is defined using an approximate fault cut-off plot constructed for the Top pre-Zechstein surface (*Fig. 5*). This surface underlies the Zechstein Supergroup and thus provides an assessment of the sub-Zechstein basement structure. The cut-off plot displays TWTT elevations of the Top pre-Zechstein surface along-strike of the CSFS along: i) the footwall fault cut-off; and ii) the axis of the major fault-parallel hanging-wall syncline, providing a proxy for a throw-length profile (*Fig. 5*). Conventional displacement-length and throw-depth profiling along with throw-contouring (e.g. Muroaka and Kamata, 1983; Childs et al., 2003; Dutton and Trudgill, 2009; Jackson et al., 2017; Lăpădat et al., 2017) are not possible along the CSFS, as all correlative pre- and syn-rift stratigraphic markers have been peneplaned off the Ringkobing-Fyn High footwall block. Although this cut-off plot does not remove the effects of post-rift inversion (e.g. Hansen et al., 2021), it is nevertheless suitable for our needs as the degree of inversion is mild relative to the degree of offset at Top pre-Zechstein level. Thus, the inversion has not significantly overprinted the first-order profile shape.

The Northern Fault is through-going and dips steeply towards the southwest. At the Top pre-Zechstein level, the maximum throw along the CSFS (~3300 ms TWT) occurs on the Northern Fault in the northwest of the study area (*Fig. 5*). Throw decreases towards the southeast where there are two 10 km long hanging-wall splays which have a maximum throw of ~1500 ms TWT (*Fig. 6*). A low amplitude and fault-parallel syncline occurs in the hanging-wall of the Northern Fault which is 8 km wide (*Fig. 6*). The syncline plunges towards the northwest, towards the region of highest throw on the CSFS and dies out to the southeast of Poul Plateau, defining a prominent sub-basin in the hanging-wall of the Northern Fault (SB1) (*Fig. 6*).

In the southern portion of the CSFS, a *ca.* 2.5 km left-stepping jog in the fault trace, and an associated block of steeply-rotated strata divides the system into two components: Southern Fault A and Southern Fault B (*Figs. 5-6*). The NNW-SSE-striking Southern Fault A has a length of approximately 28 km and a northern tip which extends for *ca.* 10 km into the footwall of the Northern Fault (*Figs. 5-6*). To the south, Southern Fault B strikes N-S and has a minimum length of 14 km (*Figs. 5-6*). Southern Faults A and B are through-going and show planar to listric geometries on time-migrated dip-section, with maximum throws of *ca.* 2500 ms TWT at the Top pre-Zechstein level (*Fig. 5*). The Southern Faults are associated with a fault-parallel hanging-wall syncline, the axial trace of which lies between 0.5-2 km basinwards of the faults. The immediate hanging-wall of the Southern Faults is compartmentalised along-strike into four 4-8.5 km long, doubly-plunging sub-basins that are elongate parallel to the fault (SB2-5) (*Fig. 6*). Of these, SB2-SB4 lie in the hanging-wall of Southern Fault A and SB5 lies in the hanging-wall of Southern Fault B (*Figs. 5-6*). A series of fault-perpendicular intra-basin highs of anticlinal geometry (H1-5) occur between the sub-basins; the axes of these highs trend approximately perpendicular to local fault strike and extend 2-3.5 km into the hanging-wall (*Fig. 6*). The centres of the sub-basins coincide with throw maxima, whereas the fault-perpendicular anticlines correspond to throw-proxy minima along-strike of Southern Faults A and B (*Figs. 5 and 6*). The fault-perpendicular folds extend across, and interfere with the fault parallel syncline, resulting in geometrically complex folding along-strike (*Fig. 6*).

Diffuse faulting around the Poul Plateau and the hanging-wall splays associated with the southern tip of the Northern Fault form a highly-faulted, breached SSE-dipping relay ramp in the regional basement high at the boundary between the Northern Fault and Southern Fault A (*Fig. 6*). The overall system is associated with a broad four-way closing hanging-wall anticline and a major along-strike throw minimum (H1 on *Figs 5 and 6*). The basal fault to the breached relay system is formed by the shallower-dipping Southern Fault A, and at both the Top pre-Zechstein and Base Callovian structural levels, the faulted terraces within the relay system are bounded by a series of predominantly synthetic, NNW-SSE to N-S-trending faults with maximum displacements of 300 ms TWT (*Fig. 6*) (Duffy et al., 2013).

4.2. Supra-Zechstein Structural Characteristics

The structural style of the supra-Zechstein syn-rift is illustrated by a TWTT structure map of the Base Callovian, a regionally-mappable and supra-Zechstein reflection which lies near to the base of the main Rift Phase 2 megasequence (*Fig. 6b*). The prominent, doubly-plunging sub-basins at Top pre-Zechstein level are also are expressed in the supra-Zechstein stratigraphy (*Fig. 6*). A broad fault-parallel syncline which plunges northwest forms the prominent sub-basin in the hanging-wall of the Northern Fault (*Figs. 6b and 7*a). The sub-basins in the hanging-wall of

Southern Faults A and B display a maximum differential relief of up to 800 ms TWT and an along-strike wavelength between fault-perpendicular anticlines of 3.5-10 km (*Figs. 6 and 8*). With the exception of a minor accumulation (~110 ms TWT) of mobile Zechstein salt at H4, mobile Zechstein salt is not preferentially thickened in the cores of supra-Zechstein fault-perpendicular anticlines (*sensu* Kane et al., 2010) (*Figs 6, 8, and 9*). As such, the differential relief of the Base Callovian hanging-wall sub-basins is not typically accentuated relative to the Top pre-Zechstein level (*Figs. 6, 8, and 9*).

4.3. Insights into Fault System Evolution from Structural Characteristics

Evidence of the segmentation and linkage history of normal faults is commonly deciphered using along-strike displacement or throw variations (e.g. Peacock and Sanderson, 1991; Anders and Schlische, 1994; Cartwright *et al*., 1995; McLeod *et al*., 2000; Wilson *et al*., 2009; Su *et al*., 2011; Kairanov et al., 2019). For the CSFS, analysis of the Top pre-Zechstein TWTT structure map and throw variations suggests that the fault system consisted of three principal components, the Northern Fault, and Southern Faults A and B (*Figs. 5 and 6*). Of these, the Northern Fault and Southern Fault A are linked by an E-W-trending jog in the fault trace near Poul Plateau (*Figs 5 and 6*). Poul Plateau is spatially coincident with H1, a fault-perpendicular anticline and regional along-strike throw minimum, and as such is interpreted as a major breached fault segment boundary (*sensu* Anders and Schlische, 1994; *Figs. 5 and 6*). Southern Faults A and B are unlinked, with the segment boundary expressed by a local decrease in the elevation of the footwall cut-off (H4) and the Igor relay ramp (*Fig. 5*). Furthermore, Southern Fault A displays three discrete along-strike throw maxima which coincide with the locations of the doubly-plunging hanging-wall synclines of SB2-SB4 (*Figs 5 and 6*). This suggests that Southern Fault A initially consisted of three precursor strands of 4-10 km in length (CSF2-4), each bounding a hanging-wall sub-basin (SB2-4) (*Figs. 5 and 6*). The fault strands linked to form the Southern Fault A observed today, with remnant segment boundaries marked by throw-minima and associated fault-perpendicular anticlines (H2-3) (*Figs. 5 and 6*).

5. Dip and Strike Variability in Structure and Stratigraphy

Having constrained the early-stage and present-day configurations of the CSFS, we now integrate seismic stratigraphic observations from along and across-strike seismic sections (*Figs. 7-9*) and thickness maps (in two-way travel-time) (*Fig. 10*) of successive intervals in the hanging-wall of the CSFS to interpret: i) the spatial and temporal evolution of the CSFS and ii) dip- and strike-oriented variability in fault system structure and hanging-wall stratal geometry. Once determined, the variations will be related to fault throw patterns, as well as the initial distribution of the Zechstein evaporites, to establish the key controls upon border fault evolution.

5.1 Triassic (~Rift Phase 1)

5.1.1 Triassic Seismic Stratigraphy

The Triassic sequence decreases in thickness both northwards towards the Poul Plateau, and eastwards towards Southern Faults A and B (*Fig. 10a*). In the hanging-wall of the Northern Fault, the seismic sequence is broadly isochronous, showing only minimal thickness variations (*Figs. 7a, 8 and 10a*). In the immediate hanging-walls of Southern Faults A and B, at least three localised, non-erosional thinner regions are present, which are elongate parallel to the faults (*Figs 7b-d, 10a*). On the Triassic thickness map, thin regions spatially coincide with synclinal sub-basins SB4 and SB5 in the hanging-walls of Southern Faults A and B, with the sequence thickening both away from the faults, and along-strike towards the intervening fault segment boundary (H4) (*Fig 10a*). The non-erosional nature of the thinning of the Triassic sequence towards the Southern Fault is best expressed at SB5, where the thickness decreases from ~850 ms TWT ~8 km away from fault to just ~350 ms TWT adjacent to Southern Fault B (*Fig. 7d*). In SB4 and SB5, this eastwards thinning is complemented by an eastward thinning of the underlying Zechstein salt (*Figs. 7c-d and 10a*). Further north, around SB2 and SB3, the Triassic thickness map does not effectively resolve any eastward thinning towards Southern Fault A (*Fig. 10a*). However, in the case of SB2, a dip-oriented seismic cross-section shows that although the Triassic sequence overall does not thin towards Southern Fault A (CSF2), the deeper portion of the Triassic sequence does thin towards the fault (*Fig. 7b*). In contrast, the overlying portion of the Triassic sequence thickens towards Southern Fault A (CSF2) (*Fig. 7b*). On an along-strike seismic section in the hanging-wall of Southern Faults A and B we observe locally thinned Triassic sequences at the centres of SB2 and SB3 which thicken towards the fault-perpendicular anticlines and fault segment boundaries (H1-H3) (*Fig. 9*). This section also shows downlap of the Triassic sequence directly onto the pre-Zechstein basement on the south-dipping syncline limb associated with SB2 (*Fig. 9*).

5.1.2 Interpretation of CSFS Structural Configuration during the Triassic Interval(~Rift Phase 1)

Stratal geometries and thickness variations in the Triassic sequence (that incorporates Rift Phase 1) suggest the CSFS consisted of five isolated components, a Northern Fault (CSF1), and Southern Faults which consisted of four isolated strands of 4 to 10 km in length (CSF2-5). Based on an estimation of the initial distribution of Zechstein salt by Duffy et al. (2013), the hanging-wall of the Northern Fault (CSF1) was free from mobile salt, whilst the hanging-wall of the Southern Fault was influenced by mobile salt which increased in thickness towards the south. We interpret that four active isolated strands (CSF2-5) in the region of the present-day Southern Faults were restricted from propagating vertically into the cover by the mobile Zechstein salt (*Fig. 11a and b*). As displacement accumulated, the supra-salt cover was folded into four fault-parallel monoclines (F2-F5), the axial traces of which were oriented broadly parallel to the tips of the underlying basement fault segments (*Fig. 11a and b*). Growth of the folds generated accommodation space between the basement and cover immediately adjacent to the displacement maxima of the basement faults, which were exploited by laterally-flowing salt present in the Southern Tail-End Graben and Salt Dome Province (*Figs. 10a and b*) (*sensu* Richardson et al., 2005; Kane et al., 2010; Wilson et al., 2023). As a result of this folding, syn-rift Triassic depocentres were offset basinwards and away from the basement faults (*Figs. 11a and b, 12a*). This configuration is expressed by the distinct zones of thinning of all (SB4 and SB5) or part (SB2) of the Triassic seismic sequence immediately adjacent to Southern Faults A and B (*Figs. 7b-d, 10a-11a and b*). In the case of SB2, the presence of a growth wedge that thickens towards Southern Fault A (CSF2) in the uppermost portion of the Triassic sequence suggests that the salt-cored fold (F2) was subsequently breached by upward propagation of basement fault CSF2 (*Fig. 7b*). Although we cannot confidently detect eastward thinning of the Triassic seismic sequence in SB3 immediately adjacent to Southern Fault A (CSF3), we do note thinning of the Triassic sequence towards the centre of SB3 and thickening towards H2 and H3 on the along-strike hanging-wall seismic cross-section. As such, infer the activity of a blind basement fault segment (CSF3) and salt-cored cover fold (F3) during at least part of the Triassic interval, that offset the depocentres offset along-strike towards H2 and H3 (*Figs 11a and b*). Overall, it is possible that the thickness variations within the Triassic sequence may have resulted from halokinesis driven by differential-loading or gravity-spreading i.e. not related to activity of the CSFS. However, the linearity of the thinner regions along Southern Faults A and B, along with the spatial correlation between the thinner regions and throw maxima along-strike of the present-day Southern Faults, suggests that CSF2-5 were blind, active drivers of halokinesis during rifting (*Figs. 9, 10a, 11a and b*).

5.2. Top Triassic to Base Callovian (~Rift Phase 2)

5.2.1 Top Triassic to Base Callovian Seismic Stratigraphy

A minimum of four main thick regions are observed which trend parallel to the CSFS and are separated along strike by thinner regions (*Fig. 10b*). Of the depocentres, one is located in the hanging-wall of the splay at the southern end of the Northern Fault, whilst a minimum of three lie in the hanging-wall of the Southern Fault (*Fig. 10b*). A single thicker region is resolved immediately adjacent to the northern portion of Southern Fault A that covers SB2 and SB3 (*Fig. 10b*). We suggest that this thick region may potentially have been composed of two subtle depocentres broadly covering SB2 and SB3 respectively, that were also influenced by a subtle high at H2 (*Fig. 10b*). Assuming this, in contrast to the underlying Triassic sequence, all five thick regions are spatially-coincident with the synclinal sub-basins (SB1-SB5) expressed on the Top pre-Zechstein and Base Callovian TWTT structure maps, with the intervening thinner regions developed above fault-perpendicular anticlines (H1-H5) (*Figs. 6, 9 and 10b*). As such, thickness variations are spatially associated with along-strike variations in present-day throw on the CSFS (*Figs. 5, 8-10b*). In map view, the depocentres are sub-circular to ellipsoidal and extend along-strike from *ca.* 2.5 to 9.5 km in length (*Fig. 10b*). Of the depocentres in the hanging-wall of the present-day Southern Faults (SB2-SB5), those in SB4 and SB5 in the southeast are thicker and more spatially extensive than those in SB2 and SB3 (*Fig. 10b*). In addition, depocentres in SB2, SB3, and SB5 display stratal wedges which thicken towards Southern Fault A (*Figs. 7b, 7d, and 10b*). The depocentre in SB4 thins towards the Southern Fault, a characteristic which we at least partly attribute to the influence of a triangular zone of mobile salt contained adjacent to the fault in the Triassic sequence that may potentially be intruded Zechstein salt or locally mobilised Triassic salt (*Figs. 7b-c and 10b*). A strike-parallel seismic traverse in the hanging-wall of the Southern Fault illustrates onlap of reflections onto the flanks of fault-perpendicular anticlines, a characteristic most pronounced within SB4 (*Fig. 9*). The seismic sequence onlaps and pinches-out onto H1, hence the immediate hanging-wall of the E-W-trending jog is interpreted as an area of non-deposition during this interval (*Fig. 9*).

5.2.2 Interpretation of CSFS Structural Configuration during the Top Triassic to Base Callovian Interval

Regional literature suggests that the Top Triassic to Base Callovian seismic sequence is composed of two tectono-stratigraphic units: i) Early Jurassic and Fjerritslev mudstones that were deposited in the time between Rift Phase 1 and Rift

Phase 2; and ii) an early Rift Phase 2-related Late Aalenian to Base Callovian unit (*Fig. 3*) (Andsbjerg and Dybkjær, 2001; Møller and Rasmussen, 2003). In addition, uplift, erosion and/or non-deposition associated with the Mid-Cimmerian Unconformity may also have influenced the interval (Andsbjerg and Dybkjær, 2001; Møller and Rasmussen, 2003), although there is no widespread expression of this within the survey (*Fig. 3*). Well data from wells G-1 and SE-Igor-1 in the south of the study area (*Fig. 2*), identify minor thicknesses (*ca.* 50-100 ms TWT) of the Fjerritslev formation within the interval, a formation which is not observed in any wells further north (see also Andsbjerg and Dybkjær, 2001). This represents, at most, 20% of the overall interval thickness. The sparse distribution of the well penetrations which identify the Mid-Cimmerian Unconformity, and lack of clear expression of the Mid-Cimmerian Unconformity at the resolution of the seismic data, means it is not possible to constrain and regionally map out the pre-rift to syn-rift megasequence boundary (for Rift Phase 2) within this sequence. However, the absence of the Fjerritslev formation within this sequence in the north, and the minor thicknesses in the south, indicates that the preserved portion of the sequence is predominantly younger than the Mid-Cimmerian Unconformity. As such, we interpret the trends of internal reflections and thickness (TWTT) variations within this sequence as a function of tectonic (Rift Phase 2) or salt-related controls. Interpreted in this way, the five thick regions located in the hanging-wall of the CSFS may represent hanging-wall depocentres associated with the five faults (CSF1-CSF5) reactivated from the Triassic structural template (*Figs. 11c-d*). Unlike in the Triassic sequence, the depocentres in SB2-SB5 thicken towards the centre of the respective fault segments (*Figs 9 and 10b*), with accommodation most likely provided by the initiation of subsidence of the salt swells which influenced the Triassic sequence (*Fig. 11c and d*).

In SB2, a stratal wedge thickens towards CSF2 indicating that CSF2 had continued to break-surface as in the later stage of the Triassic interval (*Figs 7b and 11a-d*). In SB5, the depocentre thickens towards Southern Fault B (CSF5) as opposed to during the Triassic when the sequence markedly thinned towards CSF5 (*Figs 7d and 10b*). This indicates that basement fault CSF5 likely propagated upwards and breached the overlying salt-cored cover fold (F5) during this interval (*Figs 7d, 10b, 11c and d*). Although less clear, thickening of a stratal wedge in SB3 towards CSF3 suggests CSF3 also broke surface and breached cover fold F3 during this interval.

5.3 Base Callovian to Intra-Kimmeridgian (Rift Phase 2)

5.3.1 Base Callovian to Intra-Kimmeridgian Seismic Stratigraphy

The five major depocentres within the Base Callovian to Intra-Kimmeridgian sequence are again largely spatially-coincident with the synclinal sub-basins (SB1-SB5) present on the Top pre-Zechstein and Base Callovian TWT maps, with the intervening thinner regions developed above fault-perpendicular anticlines (H1-H5) (*Figs. 6 and 10c*). As such, thickness variations are spatially associated with along-strike variations in present-day throw on the CSFS (*Figs. 8-10c*). In map view, the depocentres are again sub-circular to ellipsoid and extend for lengths along-strike from 4 to 13 km. The broader depocentre in the hanging-wall of the Northern Fault is partitioned into two sub-depocentres, one portion in the immediate hanging-wall of the main fault segment, and one associated with the southern splay (*Fig. 10c*). Of the depocentres in the hanging-wall of the Southern Faults (SB2-SB5), those in SB4 and SB5 in the southeast are by far the thickest (1000 and 1150 ms TWT respectively) and most aerially extensive. The amplitude of fault-perpendicular anticlines decreases markedly within the sequence, from a maximum relief of *ca.* 600 ms TWT at Base

Callovian horizon to *ca.* 200 ms TWT at the Intra-Kimmeridgian horizon, resulting in increasingly subtle intra-sequence thickness variations higher in the seismic sequence (*Figs. 9 and 10c*). In contrast to the underlying Top Triassic to Base Callovian depocentres, all Base Callovian to Intra-Kimmeridgian depocentres contain stratal wedges which thicken towards the CSFS (*Figs. 7 and 10c*).

A strike-parallel seismic traverse in the hanging-wall of Southern Faults A and B (*Fig. 9*) reveals onlap of the lowermost reflections within the sequence onto the fault-perpendicular anticlines (H1-H5), which is particularly evident onto H1 (*Fig. 9*). The majority of the interval drapes over the crests of the crests of H1-H5, although minor intermittent phases of onlap onto the flanks of H1-H5 are noted (*Fig. 9*). Significantly, the seismic sequence displays a stratal wedge which diverges towards the E-W-trending jog between the Northern Fault and Southern Fault A, forming a minor E-W-trending depocentre (*Fig. 9*).

5.3.2 Interpretation of CSFS Structural Configuration during the Base Callovian to Intra-Kimmeridgian Interval

Clear divergence of reflections within a stratal wedge towards the non-evaporite-influenced Northern Fault and its southern splay occurs in SB1 within this interval (*Figs 7a and 10c*). If viewed pragmatically, the Base Callovian horizon may be interpreted to represent the seismically-resolvable pre-rift to syn-rift megasequence boundary (for Rift Phase 2), although as previously mentioned, the true megasequence boundary lies within the underlying Top Triassic to Base Callovian interval. The five major depocentres identified within the Base Callovian to Intra-Kimmeridgian sequence (SB1-SB5) are interpreted to be related to the activity of three principal faults: Northern Fault (and its associated southern splay), Southern Fault A and

Southern Fault B, of which the two former are linked by an E-W-striking jog (*Fig. 11e and f*). CSF2-CSF4 are interpreted to have linked along-strike to form Southern Fault A early within this interval, based on the decreasing topographic relief of the fault-perpendicular folds upwards within the interval, a characteristic which indicates the onset of passive subsidence in the hanging-wall of Southern Fault A (e.g. Young et al., 2001). However, the fault-perpendicular anticlines (H2-H3) form persistent topographic features throughout the interval and into the Late Kimmeridgian, most likely caused by preferential load-driven withdrawal of salt from beneath the hanging-wall depocentres in fault segment centres relative to segment boundaries (*Figs. 9 and 10c*). The latest possible initiation of the E-W-trending jog and linkage of the Northern Fault to the northern tip of the newly-formed Southern Fault A is constrained to the Base Callovian, based on a faultward divergent growth wedge in the hanging-wall of the jog (*Figs. 9 and 11e and f*).

Each of the major depocentres (SB1-5) is located in the immediate hanging-wall of the present-day CSFS, suggesting the controlling faults were all surface-breaking (*Figs. 7, 10c, and 11e and f*). For the fault which controlled depocentre SB4 (i.e. CSF4), which had previously been restricted to the sub-salt basement, breaking the surface entailed upward propagation though the salt and breaching of cover fold (F4) to permit eastward migration of depocentre SB4 towards the emergent fault (*Figs. 10a-c and 11a-f*). Continued fault-controlled accommodation generation permitted the development of a thick faultward-divergent stratal wedge in SB4 (also seen in SB5) with moderate volumes of salt inferred to have withdrawn from beneath hanging-wall depocentres in SB4 and SB5 and migrated up the hanging-wall dip-slope (*Figs. 7c-d, 10c, and 11e and f*). For SB2 and SB3, we see no clear evidence of the widespread migration of salt into the hanging-wall or axially towards the cores of fault-perpendicular anticlines H1-H3 (*sensu* Kane et al., 2010). We speculate the mobile salt largely migrated into the footwall and has subsequently been eroded (e.g. Korstgård et al., 1993), or was dissolved (e.g. Clark et al., 1999).

5.4 Intra-Kimmeridgian to Late Kimmeridgian (Rift Phase 2)

5.4.1 Intra-Kimmeridgian to Late Kimmeridgian Seismic Stratigraphy

To the first order, the location and geometry of depocentres along-strike of the CSFS in the Intra-Kimmeridgian to Late Kimmeridgian seismic sequence have not changed from the underlying Base Callovian to Intra-Kimmeridgian interval (*Fig. 10d*). As such, one major northwest-thickening depocentre is located in the hanging-wall of the Northern Fault (SB1), and four depocentres within SB2-SB5 that are separated by fault-perpendicular anticlines (H1-5), occur in the hanging-wall of the Southern Faults (*Fig. 10d*). Depocentres in SB4 and SB5 in the southeast remain the thickest as in the underlying sequence (ca. 650 and 500 ms TWT respectively) (*Figs. 9 and 10d*). Differences in the geometry of depocentres relative to the Base Callovian to Intra-Kimmeridgian sequence are also recognised. For example, in the hanging-wall of Southern Fault A, the depocentre in SB4 is more elongate in a NNW-SSE-orientation (*cf. Figs. 10c and d*). In addition, although subtle, the fault-perpendicular folds did form positive topographic features throughout this interval to partition hanging-wall depocentres along-strike of Southern Faults A and B (*Figs. 9 and 10d*). In cross-section, depocentres in SB1 and SB5 contain stratal wedges which thicken broadly towards the Northern and Southern Faults respectively, thus the axes of these syn-rift depocentres lie in the immediate hanging-wall of the CSFS (*Fig. 7 and 10d*). A dip-section through the depocentre in SB5 illustrates an asymmetrical syncline with an axis which is oriented parallel to the plane of Southern Fault B (*Fig. 7d*). By contrast, the depocentres in SB2-SB4 are offset into the hanging-wall such that the sequence thins eastwards towards the Southern Fault A (*Fig. 7b-c and 10d*). The offset depocentre is best expressed in SB4, where the depocentre is offset approximately *ca.* 3.6 km from Southern Fault A and is located immediately above the Top pre-Zechstein hanging-wall cut-off (*Figs. 7c and 10d*). The SB4 depocentre is focused in the core of a symmetrical hanging-wall syncline, the eastern limb of which dips away from the fault (*Fig. 7c*). Post-Intra-Kimmeridgian reflections onlap bidirectionally onto the syncline limbs (*Fig. 7c*). In contrast to the non-vertical syncline axis at SB5, the fold in SB4 has a sub-vertical axis which is offset into the hanging-wall and located immediately above the hanging-wall cut-off of the Top pre-Zechstein horizon (*cf. Figs. 7c and 7d*).

5.4.2 Interpretation of CSFS Structural Configuration during the Intra-Kimmeridgian to Late Kimmeridgian Interval

The similarity in the location of depocentres (SB1-SB5) relative to the underlying Base Callovian to Intra-Kimmeridgian sequence indicates that they are controlled by the same configuration of faults as throughout the underlying sequence, all of which are interpreted to have been surface-breaking (*cf. Figs. 11e-f and 11g-h*). The most significant change is the shift in the location of the depocentre in SB4 away from the immediate hanging-wall of Southern Fault A (*Figs. 7c and 10d*). The depocentre is located in the core of a symmetrical growth syncline, the axis of which lies above the Top pre-Zechstein hanging-wall cut-off (*Fig. 11h*). This depocentre migration can be explained by an increase in the rate of accommodation created by withdrawal, which was focused above where the initial salt column was thickest (i.e. directly above the Top pre-Zechstein hanging-wall cut-off), compared to the rate of accommodation generation by fault-related subsidence, which was focused in the immediate hanging-wall. The evaporites withdrawn from beneath the hanging-wall depocentres migrated up the hanging-wall dip-slope to form an up-dip salt pillow and cover fold (*Fig. 7c*). It is also possible some of the salt migrated up, and was trapped adjacent to the fault plane. The chief stratigraphic implication of this redistribution of accommodation is that growth wedges thin towards active and emergent faults. In contrast, SB5 continues to thicken towards Southern Fault B, indicating the predominance of fault-related accommodation generation (*Fig. 7d*).

5.5 Late Kimmeridgian to Base Cretaceous (Rift Phase 2)

5.5.1 Late Kimmeridgian to Base Cretaceous Seismic Stratigraphy

Although the top of the Late Kimmeridgian to Base Cretaceous seismic sequence is truncated, the trends of internal reflections within the interval are used to determine the location and geometry of depocentres (*Figs. 7-9*). The seismic sequence displays less thickness variability in the hanging-wall of the CSFS than the previous intervals, with three thicker regions identified (*cf. Fig 10d and 10e*). Of these, SB1 in the hanging-wall of the Northern Fault is the most areally-extensive, and thickens markedly to the northwest, along-strike of the Northern Fault (*Figs. 8 and 10e*). A single, elongate depocentre is located in the hanging-wall of Southern Fault A, which is offset basinwards from the fault and is focused in the core of the fault-parallel syncline (*Figs. 7c and 10e*). This depocentre, which thickens to the south, is more continuous than the three distinct depocentres (SB2-SB4) observed in the underlying interval (*Figs. 9 and 10e*).

5.5.2 Interpretation of CSFS Structural Configuration during the Late Kimmeridgian to Base Cretaceous Interval

The seismic stratigraphy indicates that the configuration of the CSFS during the Late Kimmeridgian to the Base Cretaceous is similar to that throughout the underlying Intra-Kimmeridgian to Late Kimmeridgian interval (cf. *Figs. 11g-h and i-j*). One principle difference is that the relief of fault-perpendicular anticlines in the hanging-wall of Southern Fault A became negligible to absent, permitting the depocentres of SB2-SB4 to coalesce to form a continuous, elongate depocentre (*Fig. 10e*). These fault-perpendicular anticlines had remained persistent topographic features since the along-strike linkage of CSF2-CSF4 to form Southern Fault A around the Base Callovian (*Fig. 11*). Overall, the minor stratigraphic thicknesses present in the hanging-walls of Southern Faults A and B in comparison to the hanging-wall of the Northern Fault indicate relatively reduced rates of accommodation generation in the south, possibly due to reduced fault activity, or the relocation of accommodation generation due to long-wavelength regional salt redistribution (*Figs. 10e and 11*).

6. Discussion

6.1. Controls on Hanging-Wall Stratal Geometries Developed Perpendicular to Salt-Influenced Border Faults

For the Northern Fault, the hanging-wall stratal wedge that thickens towards the fault, and the broad fault-parallel hanging-wall syncline associated with SB1 are typical characteristics of border fault evolution in thick-skinned settings free from mobile salt (e.g. Prosser, 1993; Gawthorpe and Leeder, 2000; Young et al., 2001)

(*Fig. 7a*). In contrast, the more complex geometry and hanging-wall architecture of the Southern Coffee-Soil Faults indicate that mobile Zechstein salt exerts a strong control on deposition during fault growth (*Fig. 11*). Previous work documenting the relationships between salt mobility, normal faulting and hanging-wall stratigraphy suggest that dip-sections through syn-rift depocentres at various palaeo-segment centres should show predictable stratal relationships (Richardson et al., 2005; Kane et al., 2010; Wilson et al., 2023). At other thick-skinned, salt-influenced border faults, the transition from blind to emergent faulting is marked by depocentre migration towards the newly-emergent fault (Kane et al., 2010; Marsh et al. 2010). However, seismic dip-sections at various locations along-strike of the Southern Coffee-Soil Faults reveal highly-variable stratal geometries, indicating that the established models are not applicable to all settings (*Fig. 7*).

The principal difference between the Southern Coffee-Soil Faults and the Revfallet and Sleipner Faults studied by Richardson et al. (2005) and Kane et al. (2010), respectively, is that the Southern Coffee-Soil Faults do not have significant salt swells preserved in the immediate hanging-wall of the border fault, either adjacent to displacement maxima or at palaeo-segment boundaries. In the hanging-wall of the Southern Coffee-Soil Faults, previously-existing salt swells have been withdrawn and redistributed due to syn-rift sediment-loading (see Duffy et al., 2013). This load-driven withdrawal is spatially-variable, and has modified the architecture of hanging-wall depocentres along-strike (*Figs. 7b-d*). A key aspect which may influence patterns of load-induced withdrawal is spatial variability in sediment supply. For example, areas near sediment entry points may have high sediment supply and be more prone to load-induced withdrawal than sediment starved hanging-wall locations. Here we present conceptual models which address the control of competition between rates of accommodation generation by fault displacement and that created by sediment-load-induced salt withdrawal, upon the resultant stratal geometries (*Fig. 12*).

In the early stages of fault growth, a blind basement fault is impeded from penetrating and coupling with the supra-evaporite cover by pre-rift mobile salt. The overlying cover is flexed into a monocline, with a fault-parallel synclinal depocentre offset into the hanging-wall (*Fig. 12a*). Continued displacement accrual accentuates the cover monocline, generating hanging-wall accommodation in the core which varies along-strike, and which is greatest adjacent to the basement fault displacement maxima (e.g. Richardson et al., 2005; Kane et al., 2010; Wilson et al., 2023) (*Fig. 12a*). Mobile salt migrates towards and passively fills the core of the monocline, aided by gravity-driven flow down the hanging-wall dip-slope (*Fig. 12a*). The flowing salt is buttressed by the fault, with the thickest vertical column of salt located above the top pre-salt fault hanging-wall fault cut-off (i.e. basinwards of the immediate hanging-wall of the fault) (*Fig. 12a*).

Once the basement fault breaches the cover and breaks-surface, the depocentre migrates and thickens towards the emergent fault (*sensu* Kane et al., 2010; Marsh et al., 2010) (*Fig. 12b*). In the early stages of rifting, or in areas of low sediment supply, differential loading in the hanging-wall may not be sufficient to remobilise and drive away the underlying salt. However, later in the syn-rift phase, or in areas of high sediment supply, differential loading by hanging-wall stratal wedges have the potential to remobilise and drive away salt, giving rise to two end-member scenarios (*Figs. 12c and d*). Where differential sediment-loading is insufficient to initiate major withdrawal and there is only a small component of salt migration up the hanging-wall dip-slope, accommodation created by fault displacement is greater than that generated by sediment load-driven withdrawal (*Fig. 12c*). As such, the hanging-wall stratal wedges continue to thicken and diverge into the border fault, and depocentre axes are oriented parallel to the fault plane (*Fig. 12c*). This scenario is envisaged to explain the stratal geometry observed in a dip-section through the depocentre in SB5 as well as those observed by Kane et al (2010) along the Sleipner Fault Zone in the South Viking Graben (*Fig. 7d*). In contrast, where differential sediment-loading is sufficient to drive pre-rift salt up the hanging-wall dip-slope, accommodation created by load-driven withdrawal is greater than that created by fault displacement (*Fig. 12d*). As such, the depocentre shifts away from the immediate hanging-wall fault, focusing vertically above where the initial salt column was thickest and thus likely most mobile i.e. the top pre-salt hanging-wall cut-off (*Fig. 12d*). A symmetrical growth syncline develops with limbs dipping both towards and away from the fault (*Fig. 12d*). Stratal units accumulate in the growth syncline and onlap bidirectionally onto the limbs, resulting in the unusual scenario of syn-rift units thinning towards active emergent faults (*Fig. 12d*). This explains the basinward shift in the depocentre of SB4 observed above the Intra-Kimmeridgian horizon in dip-section (*Figs. 7c, 10d, 12d*). It is envisaged that this second scenario may evolve even further, with differential sediment-loading eventually depleting the salt in the immediate hanging-wall, resulting in a primary weld between the cover and basement. Once this occurs, and assuming faulting continues, fault-related subsidence will be re-established as the principal mode of accommodation generation and stratigraphic units will eventually thicken towards the fault. This is not observed above the intra-Kimmeridgian horizon in the SB4 depocentre, indicating that faulting slowed significantly or ceased immediately after the withdrawal-related accommodation generation became dominant (*Fig. 7c*).

6.2. Segmentation, Growth and Linkage of Salt-Influenced Border Faults and Implications for Along-Strike Hanging-Wall Stratal Geometry

We now explore how end-member relationships between normal faults, mobile salt and depocentre location may influence hanging-wall stratal geometries (i.e. strike-parallel sections). In *Figure 1d and f*, observations of Richardson et al., (2005) and Kane et al., (2010) are interpreted to produce conceptual along-strike hanging-wall stratigraphic sections, in a manner analogous to those developed for settings lacking mobile salt (*sensu* Schlische and Anders, 1996; Cowie et al., 2000; Morley, 2002). The contrasting geometries in each model highlights the potential for along-strike hanging-wall stratigraphic sections to be used to infer coupled fault and salt system evolution from final structural geometries (*Figs. 1d and f*). *Figure 13* summarises a new model of map-view relationships between salt migration, normal faulting and depocentre development, along with hanging-wall stratal architectures, based on observations of the Southern Coffee-Soil Faults. In the early syn-rift, salt is located in half-dome-shaped cover swells adjacent to the displacement maxima of blind basement faults (e.g. Richardson et al., 2005; Kane et al., 2010) (*Fig. 13a and b*). Syn-rift units thicken radially away from the swells, both basinwards and along-strike towards fault-perpendicular anticlines at segment boundaries (*Figs. 13a and b*). Subsequently, each of the basement faults breach the supra-salt cover folds and ruptures the surface, leading to subsidence of salt-cored swells in the centre of the fault segments (*Figs. 13c and d*). Over time, sediment-loading drives the withdrawal of salt from the swells in the centre of the fault segments, providing further accommodation so that depocentres move into the centre of the fault segments (*Figs. 13c and d*). This phase is indicated along the Southern Coffee-Soil Faults by the initiation of onlap onto the fault-perpendicular anticlines (*Fig. 9*). In contrast to the observations of Kane et al. (2010), the withdrawn salt migrates up the hanging-wall dip-slope rather than towards the cores of active fault-perpendicular anticlines at segment boundaries (*Figs. 13c and d*). Dip-parallel salt migration is supported by the following evidence: i) the absence of significant present-day salt swells at segment boundaries; ii) the absence of over-thickened late syn-rift units at palaeo-segment boundaries, which would have developed if salt had previously accumulated in the cores of fault-perpendicular anticlines and had subsequently withdrawn; and iii) the presence of salt pillows further up-dip on the hanging-wall slope (*Figs. 7c-d, 9 and 10*).

Once the border fault segments link along-strike to form one continuous fault, the fault-perpendicular anticlines may begin to passively subside in the hanging-wall, and gradually decrease in relief (*sensu* Young et al., 2001) (*Figs 13e and f*). For CSF2-CSF4, the sub-segments associated with Southern Coffee-Soil Fault A, along-strike linkage is interpreted to have occurred around the Base Callovian, yet the fault-perpendicular anticlines in the hanging-wall of Southern Fault A were preserved as apparent topographic highs until the Late Kimmeridgian (*Fig 9*). We interpret this to be a function of preferential withdrawal-related subsidence at fault segment centres relative to segment boundaries (*Figs. 9, 13e, and 13f*).

In the rift climax and into the post-rift phases, the maximum fault displacement and hence axis of subsidence of the through-going border fault is located in the centre of the fault (*Figs. 13g and h*). Sediment-loading of the immediate hanging-wall of the fault ensures that all mobile salt has withdrawn and principally migrated up the hanging-wall dip-slope, ultimately resulting in the development of a regional weld (*Figs. 13g and h*).

Although some aspects of the development of the Southern Coffee-Soil Fault described above complement aspects of established models for salt-influenced border faults (e.g. Richardson et al., 2005; Kane et al., 2010), it is the variations, and the controls on the marked shifts in depocentres through time which we seek to emphasise. Overall, our intention here has been to highlight the degree of variability and inconsistency in the inter-relationships between salt mobility, faulting and depocentre development associated with the along-strike evolution of salt-influenced faults.

6.3. Summary of Controls on Dip- and Strike-Oriented Structural Variability and Evolution of Border Fault Systems

The dip- and strike-oriented scenarios and models described here occurred contemporaneously along-strike of the Southern Coffee-Soil Faults, due to: i) spatial variations in sediment supply as determined by the distribution of sediment entry pathways into the hanging-wall such as relay zones, ii) variable displacement rates and diachronous activity on different fault segments, and iii) along-strike variations in the initial thickness of mobile salt. A key implication of the load-induced movement of salt which characterises the structural evolution of the Southern Coffee-Soil Faults, is that such styles are more likely to occur in settings where overall sediment supply is high. Therefore, fault systems at rift margins, such as the Southern Coffee-Soil Faults, are more prone to load-induced salt movement than fault systems located towards the rift axis, which are more likely to be sediment starved. This may explain the absence of major load-induced evaporite movement observed at the Revfallet and Sleipner Fault Zones as described by Richardson et al. (2005) and Kane et al. (2010).

7. Conclusions

- The CSFS initially consisted of five isolated fault strands, separated along-strike by fault-perpendicular anticlines. The isolated fault segments propagated and linked along-strike into a predominantly through-going fault prior to, or during, the Early Callovian. The tectono-stratigraphic evolution of the Southern Coffee-Soil Faults has been influenced by mobile Zechstein Supergroup salt, which increased in thickness towards the south.
- Seismic dip-sections at various locations along-strike of the Southern Coffee-Soil Faults reveal highly-variable structural geometries and depocentre shifts that established models do not adequately explain.
- During the early stages of growth of the Southern Coffee-Soil Faults, we propose that sub-cover salt swells accumulated adjacent to the displacement maxima of isolated, basement-restricted fault segments. The swells modified the relief of the depositional surface such that depocentres were offset away from the swells. Later, some of the basement-restricted fault segments linked along-strike and breached the cover to become surface-breaking. This resulted in the migration of depocentres towards the faults and, significantly, the onset of passive subsidence and burial of salt swells at fault segment centres.
- Once the faults were surface-breaking and the salt swells subsided and buried, variations in the locations and rates of accommodation generated by: i) load-driven withdrawal of salt from the swells up the hanging-wall dip-slope; and ii) fault-related subsidence, provide a critical, and hitherto neglected control upon dip- and strike-oriented variability in hanging-wall structural and stratal geometry.

- In dip-section, if sediment-loading is insufficient to initiate major withdrawal, and accommodation created by fault displacement is greater than that generated by sediment load-driven withdrawal, hanging-wall stratal wedges will continue to thicken and diverge into the border fault, and depocentre axes are oriented parallel to the fault plane. In contrast, if accommodation created by load-driven withdrawal is greater than that created by fault displacement, depocentres shift away from the immediate hanging-wall fault in dip-section, focusing vertically above where the initial salt column was thickest i.e. the top pre-salt hanging-wall cut-off. A symmetrical growth syncline develops with limbs dipping both towards and away from the fault.
- In along-strike hanging-wall sections, fault-perpendicular anticlines may be preserved as persistent features at the depositional surface even after fault segments link. This occurs when mobile salt is preferentially withdrawn from fault segment centres (i.e. where salt swells were initially located) relative to fault segment boundaries.
- Overall the dip- and strike-oriented variability along-strike of the CSFS is demonstrated to likely be a function of: i) variable displacement rates and diachronous activity on different fault segments; ii) along-strike variations in the initial thickness of mobile salt; and iii) spatial variations in sediment supply, as determined by the distribution of sediment entry pathways into the hanging-wall (eg. relay zones), a variable that may determine whether load-induced salt movement is initiated or not.

8. Acknowledgements

We thank Simon Brocklehurst, Paul Wilson, Mads Huuse and Atle Rotevatn for constructive discussions during the course of this study, along with Nancy Cottington for help with figures. Joya Tetrault and an anonymous reviewer are thanked for their constructive comments which helped improve the final version of this paper. We thank TotalEnergies (formerly Maersk Oil) for funding this PhD research project, granting permission to publish, and the help afforded by members of the Denmark Exploration Team between 2007 and 2012. We are grateful to the Dansk Undergrunds Consortium for access to seismic and well data, Schlumberger for providing access to Petrel software, and Duncan Irving for computer support. We thank the Jackson School of Geoscience, the Bureau of Economic Geology, and the Applied Geodynamics Laboratory Consortium (https://www.beg.utexas.edu/agl/sponsors) at the University of Texas at Austin for subsequent financial support that helped finalize this work. In addition, this work was able to be finalized with the help of late-stage financial support provided by the Research Council of Norway under the PETROMAKS2 programme (project number 326965) and project partners Chrysaor Norge AS and DNO Norge AS.

9. Figure Captions

Figure 1: Summary of scenarios for the evolution of non-salt- and salt-influenced border faults based on established literature. (a); (c) and (e) summarise plan-view inter-relationships between mobile salt (if present), faulting and depocentre geometry during the transition from early to late syn-rift. (b); (d) and (f) are conceptual models

of the along-strike hanging-wall architecture in both the early and late syn-rift for each scenario.

Figure 2: Structural map of the Danish Central Graben, location shown in inset, showing the location of the Coffee-Soil Fault System with respect to the main offshore faults, basins, highs, and salt structures (after Møller and Rasmussen, 2003), and the generalised salt pinchout (modified from Duffy et al., 2013). The inset displays the study area relative to the principal Jurassic structural elements and political boundaries of the North Sea Rift: CG = Central Graben; HG = Horn Graben.

Figure 3: Stratigraphic framework, showing the ages and lithologies of the formations present in the Danish Central Graben, along with regional interpretations of the major tectonic events and megasequence boundaries (after Michelsen et al., 2003; Duffy et al., 2013; Jackson et al., 2019; Patruno et al., 2022). Colour-coding of the seismic stratigraphic horizons and megasequences is continued throughout the paper.

Figure 4: (a) TWTT thickness map of the Zechstein Supergroup draped over Top pre-Zechstein basement surface. The colour bar is compressed to emphasise the major salt structures. The present-day Zechstein Supergroup thickness decreases towards the north. Dashed red lines with tick on downthrow indicate present-day Coffee-Soil Fault and dashed green line shows the Zechstein pinch-out front (modified from Duffy et al., 2013) (b) Map illustrating the approximate depositional distribution and mobility of Zechstein deposits. Note that mobile salt previously extended northwards of the present-day seismic pinch-out of mobilised Zechstein salt (parts a and b both are modified and updated from Duffy et al., 2013).

Figure. 5: (a) Trace of the CSFS (b) Profile of the fault plane, showing the TWTT elevations along the footwall cut-off of the Top pre-Zechstein horizon (TWTT) and the axis of the fault-parallel hanging-wall syncline associated with the CSFS at both the Top pre-Zechstein and Base Callovian horizons. This provides a proxy for a throw-length profile (see text). The sub-basins and components of the CSFS are labelled.

Figure 6: TWTT structure maps of (a) the Top pre-Zechstein (vertical exaggeration x5); (b) Base Callovian (vertical exaggeration x5); and (c) Late Kimmeridgian (vertical exaggeration x7.5); surfaces. Dashed red lines with tick on downthrow indicate present-day northern and southern Coffee-Soil Faults. Colour bar is compressed to highlight relief in hanging-wall. Fault-perpendicular anticline axial traces are dashed red. A series of sub-basins (SB2-5) are well-defined in the hanging-wall of the southern Coffee-Soil Fault at the Top pre-Zechstein and Base Callovian levels but are not present on the Late Kimmeridgian TWT map.

Figure 7: Uninterpreted and interpreted seismic dip-sections (i.e. oriented perpendicular to the CSFS). Each section has been flattened on a local intra-Cretaceous reflection to remove the overprinting effect of later Cenozoic inversion and is displayed at 5 x vertical exaggeration (VE). Insets display the locations of the section. (a) Dip-section through the Northern Fault and SB1. This section indicates SB1 evolved without the influence of mobile salt, with a growth wedge thickening into the Northern Fault. (b) Dip-section through Southern Fault A and SB2. The major fault-parallel anticline extends northwards and dies out to the south. Note how the

lower part of the Triassic sequence thins towards the fault, whereas the upper part of the Triassic sequence thickens towards the fault. (c) Dip-section through Southern Fault A and SB4. Note the vertical axis and symmetrical nature of the fault-parallel syncline. A southwesterly-dipping limb is developed adjacent to the fault which dips away from Southern Fault A. Note the minor Triassic thinning towards the fault, and the basinward shift in the depocentre that occurs above the Intra-Kimmeridgian. (d) Dip-section of the Southern Fault B and SB5. This section shows an asymmetrical fault-parallel syncline, the axis of which is oriented sub-parallel to the plane of the Southern Fault B. A southwesterly-dipping limb observed in SB4 is not developed here, with the syn-rift depocentres all located in the immediate hanging-wall of Southern Fault B. Note the thinning of the Triassic interval towards Southern Fault B and the thick wedge of the overlying Jurassic sequence (see also Duffy et al., 2013). Seismic polarity cartoons are courtesy of Agile Scientific (https://agilescientific.com/blog/2012/4/5/polarity-cartoons.html).

Figure 8: Uninterpreted and interpreted strike-parallel seismic traverse in the hanging-wall of the Northern Fault (location shown in inset) at VE x5. The section line is located away from the effects of splay faults and contains a single, large depocentre, with units generally thickening towards the axis of SB1 in the northwest. The section is flattened on an intra-Cretaceous horizon to remove the effect of late-stage inversion. Seismic polarity cartoon is courtesy of Agile Scientific (https://agilescientific.com/blog/2012/4/5/polarity-cartoons.html).

Figure 9: Uninterpreted and interpreted strike-parallel seismic traverse in the hanging-wall of Southern Faults A and B, taken along the axis of the major hanging-

wall syncline (location shown in inset) (VE x5). Section (presented unflattened) displays only a mild degree of inversion that does not overprint the overall thickness variations and geometries in the Triassic and Jurassic sequences. The section highlights a series of four major depocentres along-strike of the Southern Fault (SB2-SB5), bounded by fault-perpendicular anticlines (H1-H5). The fault-perpendicular folds, which also affect the Top pre-Zechstein horizon, die out vertically by the Late Kimmeridgian. Note the thinning of the Triassic interval into the centre of the sub-basins (most accentuated at SB2 and SB3) and the compensational overthickening of the overlying sequence. Seismic polarity cartoon is courtesy of Agile Scientific (https://agilescientific.com/blog/2012/4/5/polarity-cartoons.html).

Figure 10: Maps displaying the thickness variations (in TWTT) of key tectono-stratigraphic units across the study area. (a) Triassic (Rift Phase 1); (b) Top Triassic to Base Callovian (Rift Phase 2); (c) Base Callovian to Intra-Kimmeridgian (Rift Phase 2); (d) Intra-Kimmeridgian to Late Kimmeridgian (Rift Phase 2); and (e) Late Kimmeridgian to Base Cretaceous (Rift Phase 2). Note that the colour maps showing thickness variations within an interval are draped over the present-day structure of the basal surface of the given interval (structural contours of which are shown in black). These maps highlight how depocentres relate to structural features. Dashed red line indicates the Coffee-Soil Fault, with a tick on the downthrow.

Figure 11: Evolution of fault activity and salt migration pathway maps for basement and cover faults respectively. For each interval, the top figure displays the distributions of active basement faults, along with the locations of mobile salt (thicker salt indicated by a darker shade of orange) and inferred migration pathways (yellow

arrows, with bigger arrows indicating higher salt flux). The lower figures shown at each interval document the configuration of active cover faults, folds and associated depocentres (cover monoclines shown with red arrows; thicker depocentres indicated by a darker shade of blue). Dashed lines and question marks indicate uncertainty of interpretation. Please note that in a) and b) CSF2 is depicted as blind basement fault that is overlain by cover monocline F2. This represents our interpretation of the configuration during the earlier part of the Triassic. However, later in the Triassic CSF2 breached the surface and the depocentre thickened towards CSF2.

Figure 12: Synoptic diagram illustrating controls on dip-section variability in hanging-wall tectono-stratigraphy throughout the evolution of a salt-influenced border fault system. (a) Faulting restricted to the pre-salt basement and a forced cover monocline develops in the supra-salt cover. (b) Early syn-rift scenario after the basement fault breaches the cover; the depocentre remains in the immediate hanging-wall of the fault. (c) and (d) Depict two alternative scenarios for the late syn-rift evolution. (c) Illustrates a scenario where accommodation space created by fault displacement is greater than that created by load-driven withdrawal focused above the Top pre-salt hanging-wall cut-off (where salt is thickest as likely most mobile); the depocentre axis remains adjacent to the border fault. (d) Portrays an alternative scenario where accommodation space created by load-driven withdrawal outpaces that created by fault displacement; the depocentre shifts basinwards to above the Top pre-salt hanging-wall cut-off. Note the symmetrical hanging-wall syncline geometry and thinning of the syn-rift towards the active fault. Salt is shown in red, sediments in shades of purple (broadly representing Triassic age sediments) and blue (broadly representing Jurassic age sediments).

Figure 13: Synoptic model based on observations from the Southern Coffee-Soil Faults, summarising i) map-view relationships between salt mobility, faulting and depocentre geometry throughout border fault evolution (a, c, e, and g); ii) the development of along-strike hanging-wall architecture in hanging-wall section profiles (b, d, f, and h). Salt is shown in red, sediments in shades of purple (broadly representing Triassic age sediments) and blue (broadly representing Jurassic age sediments).

10. References

Anders, M.H. & Schlische, R.W. (1994) Overlapping Faults, Intrabasin Highs, and the Growth of Normal Faults. *Journal of Geology*, 102, 165-180, DOI: 10.1086/629661.

Andsbjerg, J. & Dybkjær, K. (2003) Sequence Stratigraphy of the Jurassic of the Danish Central Graben. *Geological Survey of Denmark and Greenland Bulletin*, 1, 265-300, DOI: 10.34194/geusb.v1.4675

Bruhn, R. & Vagle, K. (2005) Relay Ramp Evolution and Mass Flow Deposition (Upper Kimmeridgian-Lower Volgian) in the Tail End Graben, Danish North Sea. *Basin Research*, 17, 551-567, DOI: 10.1111/j.1365-2117.2005.00276.x

Cartwright, J.A. (1987) Transverse Structural Zones in Continental Rifts-an Example from the Danish Sector of the North Sea. *Petroleum Geology of North West Europe. Graham & Trotman, London*, 441, 452.

Cartwright, J.A. (1989) The Kinematics of Inversion in the Danish Central Graben. *Geological Society London Special Publications*, 44, 153, DOI: 10.1144/GSL.SP.1989.044.01.10

Cartwright, J. (1991) The Kinematic Evolution of the Coffee Soil Fault. *Geological Society London Special Publications*, 56, 29, DOI: 10.1144/GSL.SP.1991.056.01.03

Cartwright, J.A., Trudgill, B.D. & Mansfield, C.S. (1995) Fault Growth by Segment Linkage - an Explanation for Scatter in Maximum Displacement and Trace Length Data from the Canyonlands Grabens of Se Utah. *Journal of Structural Geology*, 17, 1319-1326. DOI: 10.1016/0191-8141(95)00033-A

Childs, C., Nicol, A., Walsh, J.J. & Watterson, J. (2003) The Growth and Propagation of Synsedimentary Faults. *Journal of Structural Geology*, 25, 633-648, DOI: 10.1016/S0191-8141(02)00054-8

Clark, J.A., Cartwright, J.A. & Stewart, S.A. (1999) Mesozoic Dissolution Tectonics on the West Central Shelf, UK Central North Sea. *Marine and Petroleum Geology*, 16, 283-300, DOI: 10.1016/S0264-8172(98)00040-3

Cowie, P.A., Gupta, S. & Dawers, N.H. (2000) Implications of Fault Array Evolution for Synrift Depocentre Development: Insights from a Numerical Fault Growth Model. *Basin Research*, 12, 241-261, DOI: 10.1046/j.1365-2117.2000.00126.x

Dooley, T., McClay, K., Hempton, M. & Smit, D. (2005). *Salt Tectonics above Complex Basement Extensional Fault Systems: Results from Analogue Modelling*. Geological Society, London, Petroleum Geology Conference series, Geological Society of London, DOI: 10.1144/0061631

Duffy, O.B., Gawthorpe, R.L., Docherty, M. & Brocklehurst, S.H. (2013) Mobile Evaporite Controls on the Structural Style and Evolution of Rift Basins: Danish Central Graben, North Sea. *Basin Research*, 25, 310-330. DOI: 10.1111/bre.12000

Dutton, D.M. & Trudgill, B.D. (2009) Four-Dimensional Analysis of the Sembo Relay System, Offshore Angola: Implications for Fault Growth in Salt-Detached Settings. *AAPG Bulletin*, 93, 763-794. DOI: 10.1306/02230908094

Erratt, D. (1993). *Relationships between Basement Faulting, Salt Withdrawal and Late Jurassic Rifting, UK Central North Sea*, Geological Society of London. DOI: 10.1144/0041211

Ford, M., de Veslud, C.L.C. & Bourgeois, O. (2007) Kinematic and Geometric Analysis of Fault-Related Folds in a Rift Setting: The Dannemarie Basin, Upper Rhine Graben, France. *Journal of Structural Geology*, 29, 1811-1830. DOI: 10.1016/j.jsg.2007.08.001

Gawthorpe, R.L. & Leeder, M.R. (2000) Tectono-Sedimentary Evolution of Active Extensional Basins. *Basin Research*, 12, 195-218. DOI: 10.1046/j.1365-2117.2000.00121.x

Ge, Z.Y., Gawthorpe, R.L., Rotevatn, A. & Thomas, M.B. (2017) Impact of Normal Faulting and Pre-Rift Salt Tectonics on the Structural Style of Salt-Influenced Rifts: The Late Jurassic Norwegian Central Graben, North Sea. *Basin Research*, 29, 674-698. DOI: 10.1111/bre.12219

Gowers, M.B. & Saeboe, A. (1985) On the Structural Evolution of the Central Trough in the Norwegian and Danish Sectors of the North Sea. *Marine and Petroleum Geology*, 2, 298-318, DOI: 10.1016/0264-8172(85)90026-1

Hansen, T.H., Clausen, O.R. & Andresen, K.J. (2020) Thick-and Thin-Skinned Basin Inversion in the Danish Central Graben, North Sea–the Role of Deep Evaporites and Basement Kinematics. *Solid Earth Discussions*, 1-39, DOI: 10.5194/se-12-1719-2021

Hodgson, N.A., Farnsworth, J. & Fraser, A.J. (1992) Salt-Related Tectonics, Sedimentation and Hydrocarbon Plays in the Central Graben, North-Sea, UKCS. *Exploration Britain*, 67, 31-63, DOI: 10.1144/GSL.SP.1992.067.01.03

Jackson, C.A.-L. & Rotevatn, A. (2013) 3D Seismic Analysis of the Structure and Evolution of a Salt-Influenced Normal Fault Zone: A Test of Competing Fault Growth Models. *Journal of Structural Geology*, 54, 215-234, DOI: 10.1016/j.jsg.2013.06.012

Jackson, C.A.L. & Lewis, M.M. (2015) Structural Style and Evolution of a Salt-Influenced Rift Basin Margin; the Impact of Variations in Salt Composition and the Role of Polyphase Extension. *Basin Research*, DOI: 10.1111/bre.12099

Jackson, C.A.L., Bell, R.E., Rotevatn, A. & Tvedt, A.B.M. (2017) Techniques to Determine the Kinematics of Synsedimentary Normal Faults and Implications for Fault Growth Models. *Geometry and Growth of Normal Faults*, 439, 187-217. DOI: 10.1144/Sp439.22

Jackson, C.-L. & Stewart, S. (2017) Composition, Tectonics, and Hydrocarbon Significance of Zechstein Supergroup Salt on the United Kingdom and Norwegian Continental Shelves: A Review. In: *Permo-Triassic Salt Provinces of Europe, North Africa and the Atlantic Margins*, 175-201. DOI: 10.1016/B978-0-12-809417-4.00009-4

Jackson, C.A.L., Elliott, G.M., Royce-Rogers, E., Gawthorpe, R.L. & Aas, T.E. (2019) Salt Thickness and Composition Influence Rift Structural Style, Northern North Sea, Offshore Norway. *Basin Research*, 31, 514-538. DOI: 10.1111/bre.12332

Janecke, S.U., Vandenburg, C.J. & Blankenau, J.J. (1998) Geometry, Mechanisms and Significance of Extensional Folds from Examples in the Rocky Mountain Basin and Range Province, Us A. *Journal of Structural Geology*, 20, 841-856, DOI: 10.1016/S0191-8141(98)00016-9

Kairanov, B., Marin, D., Escalona, A. & Cardozo, N. (2019) Growth and Linkage of a Basin-Bounding Fault System: Insights from the Early Cretaceous Evolution of the Northern Polhem Subplatform, SW Barents Sea. *Journal of Structural Geology*, 124, 182-196. DOI: 10.1016/j.jsg.2019.04.014

Kane, K.E., Jackson, C.A.L. & Larsen, E. (2010) Normal Fault Growth and Fault-Related Folding in a Salt-Influenced Rift Basin: South Viking Graben, Offshore Norway. *Journal of Structural Geology*, 32, 490-506. DOI: 10.1016/j.jsg.2010.02.005

Karlo, J.F., van Buchem, F.S.P., Moen, J. & Milroy, K. (2014) Triassic-Age Salt Tectonics of the Central North Sea. *Interpretation-A Journal of Subsurface Characterization*, 2, DOI: 10.1190/INT-2014-0032.1

Korstgård, J.A., Lerche, I., Mogensen, T.E. & Thomsen, R.O. (1993) Salt and Fault Interactions in the Northeastern Danish Central Graben: Observations and Inferences. *Bulletin of the Geological Society of Denmark*, 40, 4.

Lăpădat, A., Imber, J., Yielding, G., Iacopini, D., McCaffrey, K.J., Long, J.J. & Jones, R.R. (2017) Occurrence and Development of Folding Related to Normal Faulting within a Mechanically Heterogeneous Sedimentary Sequence: A Case Study from Inner Moray Firth, UK. *Geological Society, London, Special Publications*, 439, 373-394. DOI: 10.1144/SP439.18

Lewis, M.M., Jackson, C.A.L. & Gawthorpe, R.L. (2013) Salt-Influenced Normal Fault Growth and Forced Folding: The Stavanger Fault System, North Sea. *Journal of Structural Geology*, 54, 156-173. DOI: 10.1016/j.jsg.2013.07.015

Marsh, N., Imber, J., Holdsworth, R.E., Brockbank, P. & Ringrose, P. (2010) The Structural Evolution of the Halten Terrace, Offshore Mid-Norway: Extensional Fault Growth and Strain Localisation in a Multi-Layer Brittle–Ductile System. *Basin Research*, 22, 2, 195-214, DOI: 10.1111/j.1365-2117.2009.00404.x

McLeod, A.E., Dawers, N.H. & Underhill, J.R. (2000) The Propagation and Linkage of Normal Faults: Insights from the Strathspey-Brent-Statfjord Fault Array, Northern North Sea. *Basin Research*, 12, 263-284. DOI: 10.1046/j.1365-2117.2000.00124.x

Michelsen, O., Nielsen, L.H., Johannessen, P.N., Andsbjerg, J. & Surlyk, F. (2003) Jurassic Lithostratigraphy and Stratigraphic Development Onshore and Offshore Denmark. *Geological Survey of Denmark and Greenland (GEUS) Bulletin*, 1, 145-216, DOI: 10.34194/geusb.v1.4651

Moller, J.J. (1986) *Seismic Structural Mapping of the Middle and Upper Jurassic in the Danish Central Trough*. I kommission hos CA Reitzels forlag.

Møller, J.J. & Rasmussen, E.S. (2003) Middle Jurassic–Early Cretaceous Rifting of the Danish Central Graben. *Geological Survey of Denmark and Greenland Bulletin*, 1, 247-264, DOI: 10.34194/geusb.v1.4654

Morley, C.K. (1999) Patterns of Displacement Along Large Normal Faults: Implications for Basin Evolution and Fault Propagation, Based on Examples from East Africa. *AAPG Bulletin*, 83, 613-634.

Morley, C.K. (2002) Evolution of Large Normal Faults: Evidence from Seismic Reflection Data. *AAPG Bulletin*, 86, 961-978.

Muraoka, H. & Kamata, H. (1983) Displacement Distribution Along Minor Fault Traces. *Journal of Structural Geology*, 5, 483-495. DOI: 10.1016/0191-8141(83)90054-8

Nalpas, T. & Brun, J.P. (1993) Salt Flow and Diapirism Related to Extension at Crustal-Scale. *Tectonophysics*, 228, 349-362. DOI: 10.1016/0040-1951(93)90348-N

Nixon, C.W., McNeill, L.C., Bull, J.M., Bell, R.E., Gawthorpe, R.L., Henstock, T.J., Christodoulou, D., Ford, M., Taylor, B., Sakellariou, D., Ferentinos, G., Papatheodorou, G., Leeder, M.R., Collier, R.E.L.I., Goodliffe, A.M., Sachpazi, M. & Kranis, H. (2016) Rapid Spatiotemporal Variations in Rift Structure During Development of the Corinth Rift, Central Greece. *Tectonics*, 35, 1225-1248. DOI: 10.1002/2015tc004026

Patruno, S., Kombrink, H. & Archer, S.G. (2022) Cross-Border Stratigraphy of the Northern, Central and Southern North Sea: A Comparative Tectono-Stratigraphic Megasequence Synthesis. *Geological Society London Special Publications,* 494, 13, DOI: 10.1144/SP494-2020-228

Peacock, D.C.P. & Sanderson, D.J. (1991) Displacements, Segment Linkage and Relay Ramps in Normal-Fault Zones. *Journal of Structural Geology*, 13, 721. DOI: 10.1016/0191-8141(91)90033-F

Prosser, S. (1993) Rift-Related Linked Depositional Systems and Their Seismic Expression. *Geological Society London Special Publications*, 71, 35, DOI: 10.1144/GSL.SP.1993.071.01.03

Rank-Friend, M. & Elders, C.F. (2004) The Evolution and Growth of Central Graben Salt Structures, Salt Dome Province, Danish North Sea. *Geological Society London Memoirs*, 29, 149, DOI: 10.1144/GSL.MEM.2004.029.01.15

Rasmussen, E.S. (2009) Neogene Inversion of the Central Graben and Ringkobing-Fyn High, Denmark. *Tectonophysics*, 465, 84-97. DOI: 10.1016/j.tecto.2008.10.025

Richardson, N.J., Underhill, J.R. & Lewis, G. (2005) The Role of Evaporite Mobility in Modifying Subsidence Patterns During Normal Fault Growth and Linkage, Halten Terrace, Mid-Norway. *Basin Research*, 17, 203-223. DOI: 10.1111/j.1365-2117.2005.00250.x

Schlische, R.W. (1995) Geometry and Origin of Fault-Related Folds in Extensional Settings. *AAPG Bulletin-American Association of Petroleum Geologists*, 79, 1661-1678. DOI: 10.1306/7834DE4A-1721-11D7-8645000102C1865D

Serck, C.S. & Braathen, A. (2019) Extensional Fault and Fold Growth: Impact on Accommodation Evolution and Sedimentary Infill. *Basin Research*, 31, 967-990. DOI: 10.1111/bre.12353

Soto, R., Casas-Sainz, A.M. & del Rio, P. (2007) Geometry of Half-Grabens Containing a Mid-Level Viscous Decollement. *Basin Research*, 19, 437-450. DOI: 10.1111/j.1365-2117.2007.00328.x

Stemmerik, L., Ineson, J.R. & Mitchell, J.G. (2000) Stratigraphy of the Rotliegend Group in the Danish Part of the Northern Permian Basin, North Sea. *Journal of the Geological Society*, 157, 1127-1136. DOI: 10.1144/jgs.157.6.1127

Stewart, S. (2014) Detachment-Controlled Triangle Zones in Extension and Inversion Tectonics. *Interpretation*. DOI: 10.1190/INT-2014-0026.1

Stewart, S.A., Harvey, M.J., Otto, S.C. & Weston, P.J. (1996) Influence of Salt on Fault Geometry: Examples from the UK Salt Basins. *Geological Society London Special Publications*, 100, 175, DOI: 10.1144/GSL.SP.1996.100.01.12

Stewart, S.A., Ruffell, A.H. & Harvey, M.J. (1997) Relationship between Basement-Linked and Gravity-Driven Fault Systems in the UKCS Salt Basins. *Marine and Petroleum Geology*, 14, 579-602, DOI: 10.1016/S0264-8172(97)00008-1

Stewart, S.A. & Clark, J.A. (1999). *Impact of Salt on the Structure of the Central North Sea Hydrocarbon Fairways*, Geological Society Pub House, DOI: 10.1144/0050179

Su, J.B., Zhu, W.B., Wei, J., Xu, L.M., Yang, Y.F., Wang, Z.Q. & Zhang, Z.Y. (2011) Fault Growth and Linkage: Implications for Tectonosedimentary Evolution in the Chezhen Basin of Bohai Bay, Eastern China. *AAPG Bulletin*, 95, 1-26, DOI: 10.1306/06301009207

Sundsbø, G.O. & Megson, J.B. (1993) Structural Styles in the Danish Central Graben. *Petroleum geology of Northwest Europe: proceedings of the 4th conference*, 1255–1267, DOI: 10.1144/0041255

Taylor, J. (1998) Upper Permian—Zechstein. *Petroleum Geology of the North Sea: Basic concepts and recent advances*, 174-211, DOI: 10.1002/9781444313413.ch6

Tvedt, A.B.M., Rotevatn, A., Jackson, C.A.L., Fossen, H. & Gawthorpe, R.L. (2013) Growth of Normal Faults in Multilayer Sequences: A 3D Seismic Case Study from the Egersund Basin, Norwegian North Sea. *Journal of Structural Geology*, 55, 1-20, DOI: 10.1016/j.jsg.2013.08.002

Vejbæk, O.V. & Andersen, C. (2002) Post Mid-Cretaceous Inversion Tectonics in the Danish Central Graben–Regionally Synchronous Tectonic Events. *Bulletin of the Geological Society of Denmark*, 49, 129–144.

Wilson, E.P., Granado, P., Santolaria, P., Ferrer, O. & Muñoz, J.A. (2023) Inversion of Transfer Zones in Salt-Bearing Extensional Systems: Insights from Analogue Modeling. *EGUsphere*, 2023, 1-38. DOI: 10.5194/egusphere-2022-1461

Wilson, P., Hodgetts, D., Rarity, F., Gawthorpe, R.L. & Sharp, I.R. (2009) Structural Geology and 4d Evolution of a Half-Graben: New Digital Outcrop Modelling Techniques Applied to the Nukhul Half-Graben, Suez Rift, Egypt. *Journal of Structural Geology*, 31, 328-344. DOI: 10.1016/j.jsg.2008.11.013

Wilson, P., Elliott, G.M., Gawthorpe, R.L., Jackson, C.A.L., Michelsen, L. & Sharp, I.R. (2013) Geometry and Segmentation of an Evaporite-Detached Normal Fault Array: 3D Seismic Analysis of the Southern Bremstein Fault Complex, Offshore Mid-Norway. *Journal of Structural Geology*, 51, 74-91. DOI: 10.1016/j.jsg.2013.03.005

Withjack, M.O. & Callaway, S. (2000) Active Normal Faulting beneath a Salt Layer: An Experimental Study of Deformation Patterns in the Cover Sequence. *AAPG Bulletin-American Association of Petroleum Geologists*, 84, 627-651, DOI: 10.1306/C9EBCE73-1735-11D7-8645000102C1865D

Young, M.J., Gawthorpe, R.L. & Hardy, S. (2001) Growth and Linkage of a Segmented Normal Fault Zone; the Late Jurassic Murchison-Statfjord North Fault, Northern North Sea. *Journal of Structural Geology*, 23, 1933-1952. DOI: 10.1016/S0191-8141(01)00038-4

Ziegler, P.A. (1975) Geologic Evolution of North-Sea and Its Tectonic Framework. *AAPG Bulletin-American Association of Petroleum Geologists*, 59, 1073-1097, DOI: 10.1306/83D91F2E-16C7-11D7-8645000102C1865D

Ziegler, P.A. (1990) Tectonic and Palaeogeographic Development of the North Sea Rift System. *Tectonic Evolution of the North Sea Rifts. Clarendon Press, Oxford*, 1–36.

Fig 1

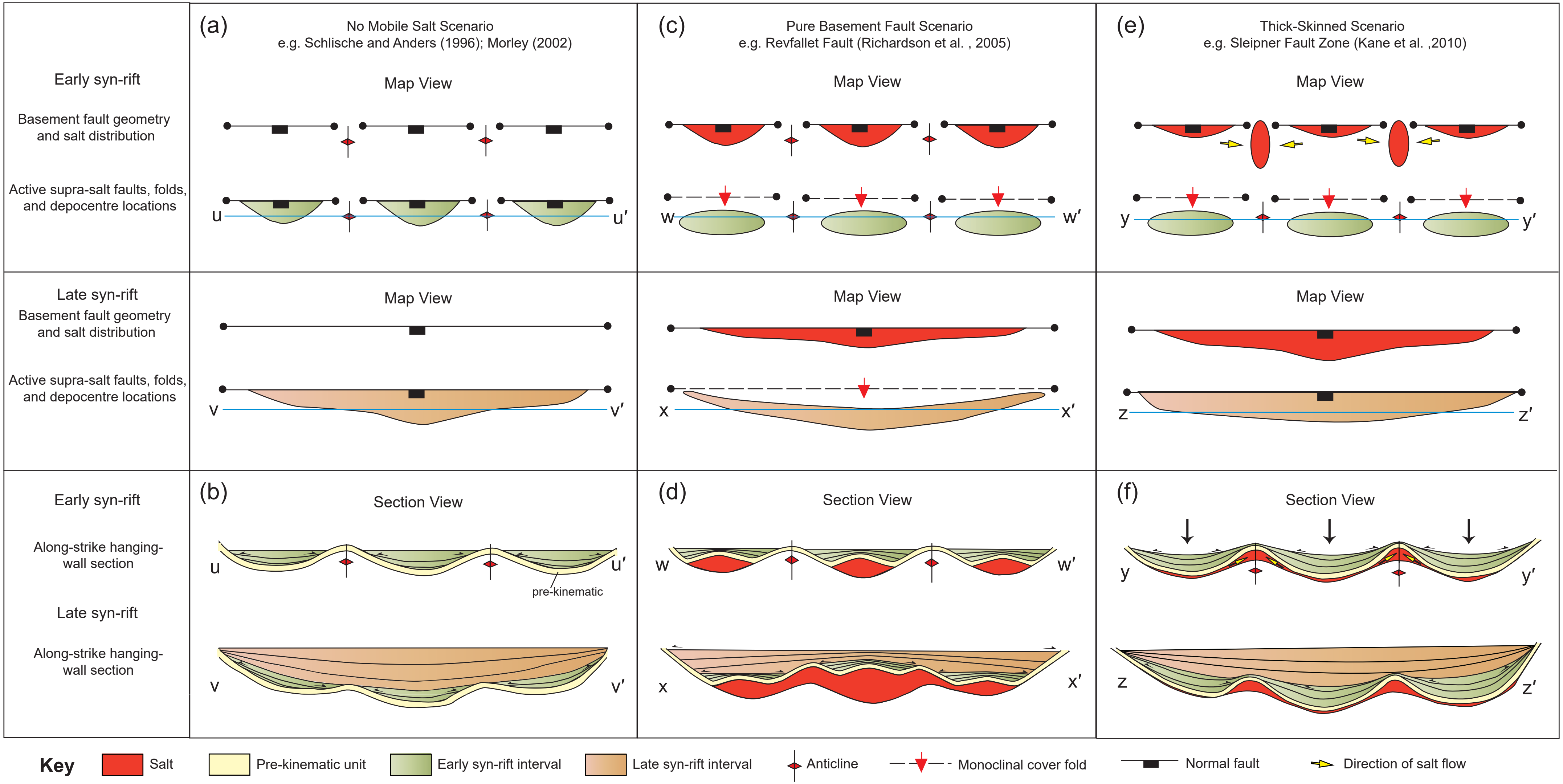

Early syn-rift
Basement fault geometry and salt distribution
Active supra-salt faults, folds, and depocentre locations
Late syn-rift
Basement fault geometry and salt distribution
Active supra-salt faults, folds, and depocentre locations
Early syn-rift
Along-strike hanging-wall section
Late syn-rift
Along-strike hanging-wall section
(a)
No Mobile Salt Scenario
e.g. Schlische and Anders (1996); Morley (2002)
Map View
u
u′
Map View
v
v′
(b)
Section View
u
u′
pre-kinematic
v
v′
(c)
Pure Basement Fault Scenario
e.g. Revfallet Fault (Richardson et al. , 2005)
Map View
w
w′
Map View
x
x′
(d)
Section View
w
w′
x
x′
(e)
Thick-Skinned Scenario
e.g. Sleipner Fault Zone (Kane et al. ,2010)
Map View
y
y′
Map View
z
z′
(f)
Section View
y
y′
z
z′
Key
Salt
Pre-kinematic unit
Early syn-rift interval
Late syn-rift interval
Anticline
Monoclinal cover fold
Normal fault
Direction of salt flow

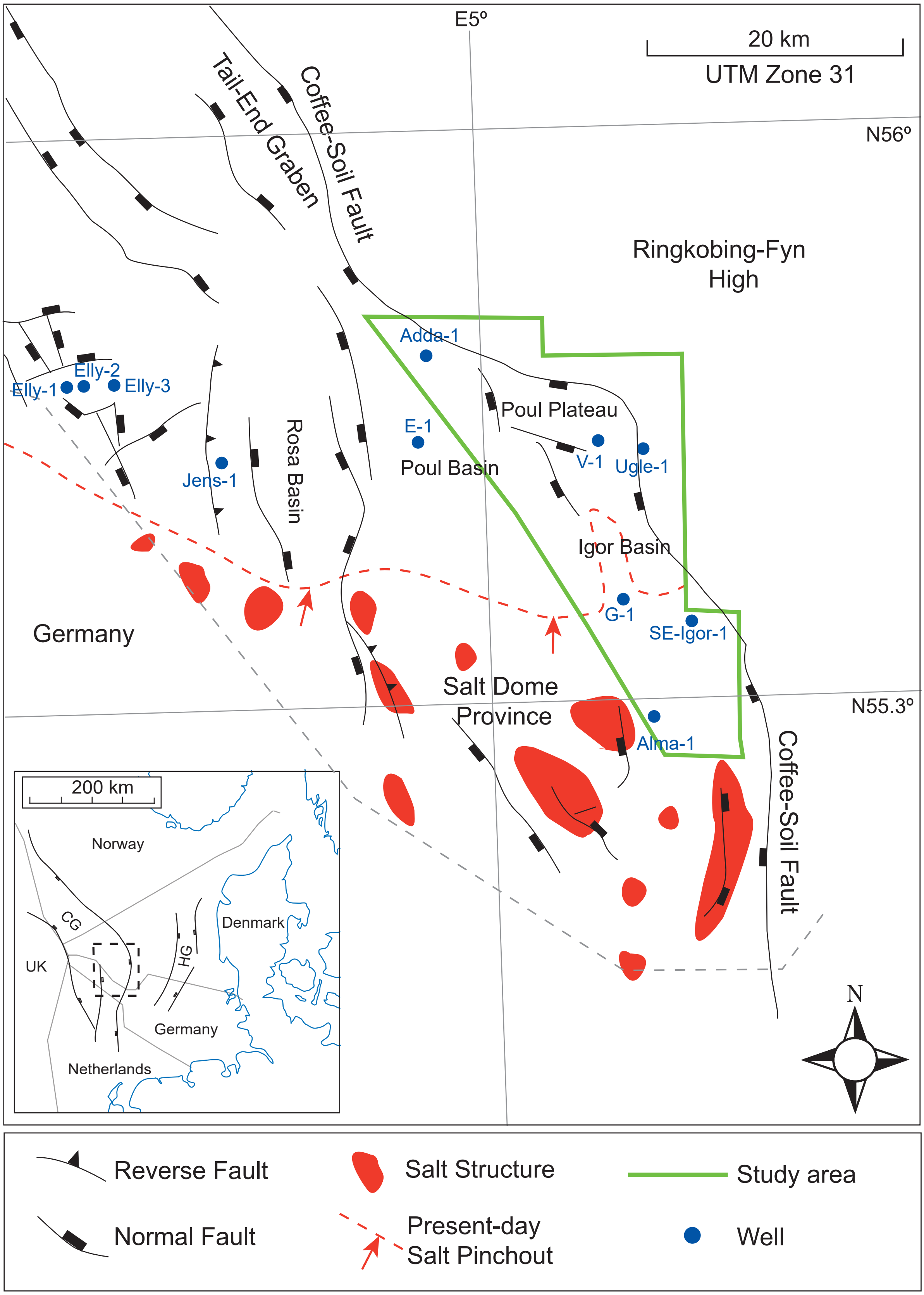

E5º
20 km
UTM Zone 31
N56º
Tail-End Graben
Coffee-Soil Fault
Ringkobing-Fyn
High
Adda-1
Elly-2
Elly-1
Elly-3
Poul Plateau
E-1
V-1
Ugle-1
Poul Basin
Jens-1
Rosa Basin
Igor Basin
G-1
SE-Igor-1
Germany
Salt Dome
Province
N55.3º
Alma-1
Coffee-Soil Fault
200 km
Norway
CG
Denmark
UK
HG
Germany
Netherlands
N
Reverse Fault
Normal Fault
Salt Structure
Present-day
Salt Pinchout
Study area
Well

Fig 2

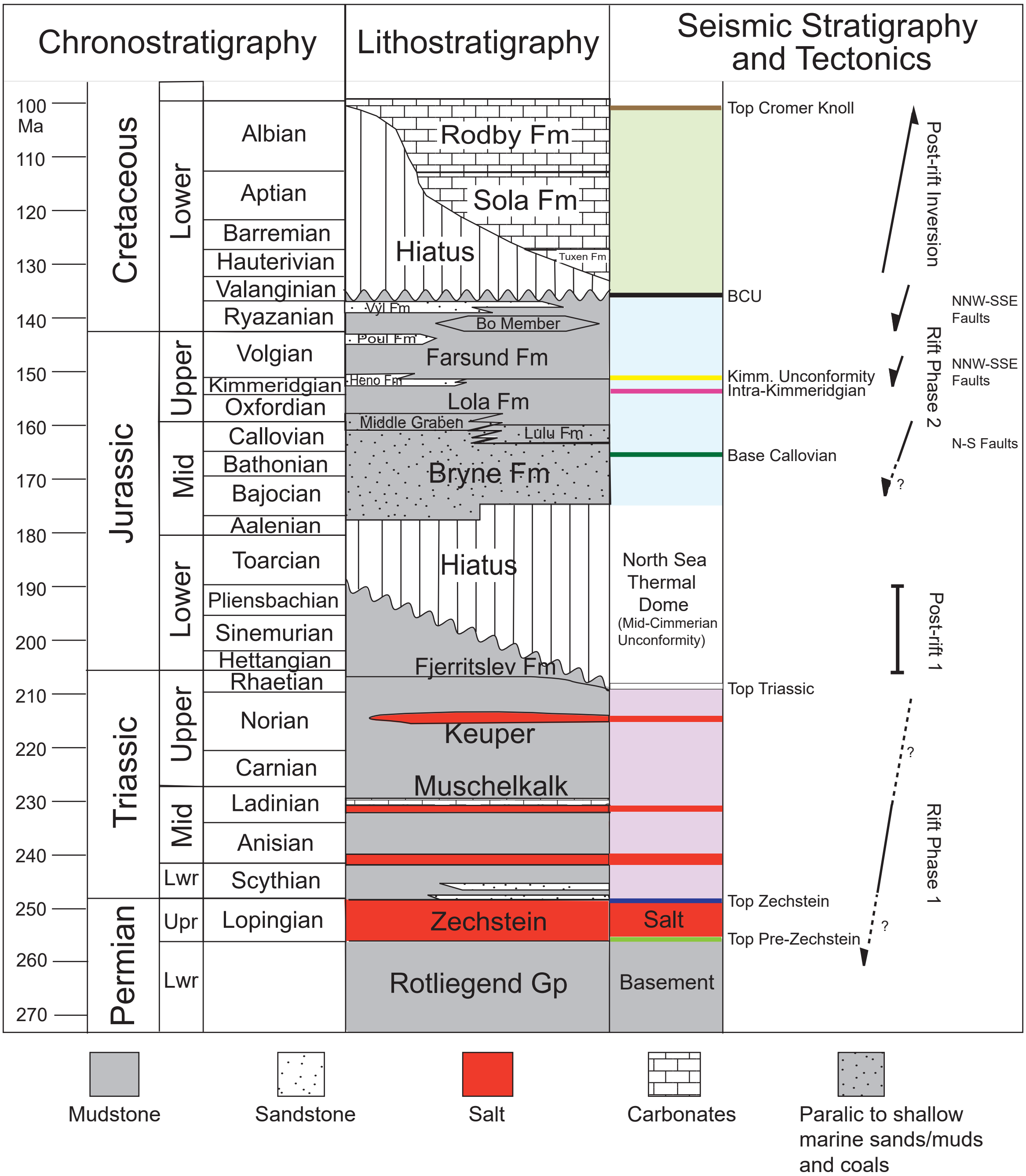

Chronostratigraphy
Lithostratigraphy
Seismic Stratigraphy and Tectonics
100 Ma
110
120
130
140
150
160
170
180
190
200
210
220
230
240
250
260
270
Cretaceous
Jurassic
Triassic
Permian
Lower
Upper
Mid
Lower
Upper
Mid
Lwr
Upr
Lwr
Albian
Aptian
Barremian
Hauterivian
Valanginian
Ryazanian
Volgian
Kimmeridgian
Oxfordian
Callovian
Bathonian
Bajocian
Aalenian
Toarcian
Pliensbachian
Sinemurian
Hettangian
Rhaetian
Norian
Carnian
Ladinian
Anisian
Scythian
Lopingian
Rodby Fm
Sola Fm
Hiatus
Tuxen Fm
Vyl Fm
Bo Member
Poul Fm
Farsund Fm
Heno Fm
Lola Fm
Middle Graben
Lulu Fm
Bryne Fm
Hiatus
Fjerritslev Fm
Keuper
Muschelkalk
Zechstein
Rotliegend Gp
North Sea Thermal Dome
(Mid-Cimmerian Unconformity)
Salt
Basement
Top Cromer Knoll
BCU
Kimm. Unconformity
Intra-Kimmeridgian
Base Callovian
Top Triassic
Top Zechstein
Top Pre-Zechstein
Post-rift Inversion
Rift Phase 2
Post-rift 1
Rift Phase 1
NNW-SSE Faults
NNW-SSE Faults
N-S Faults
?
Mudstone
Sandstone
Salt
Carbonates
Paralic to shallow marine sands/muds and coals

Fig 3

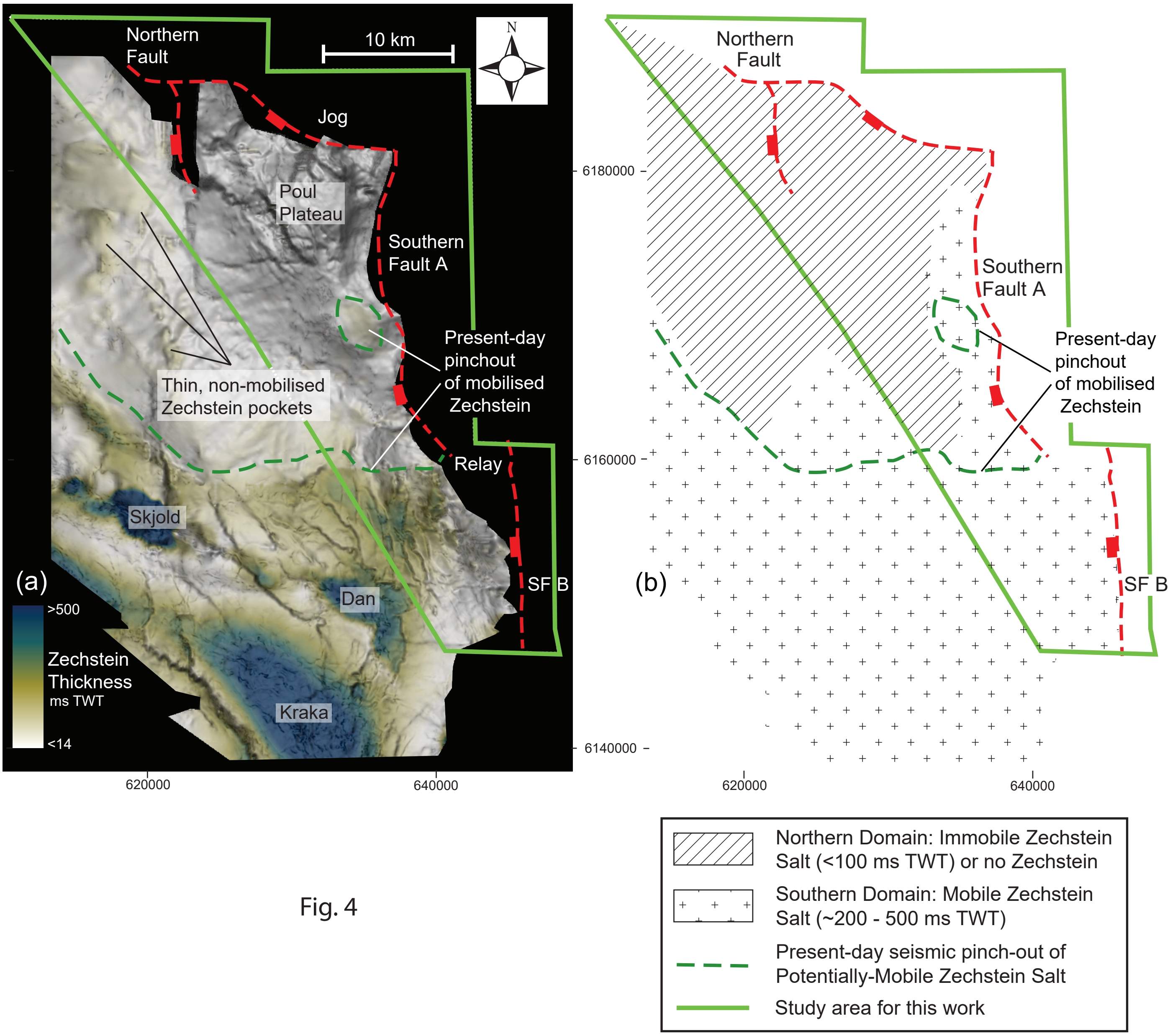

Northern Fault
10 km
N
Jog
Poul Plateau
Southern Fault A
Present-day pinchout of mobilised Zechstein
Thin, non-mobilised Zechstein pockets
Relay
Skjold
SF B
(a)
>500
Zechstein Thickness ms TWT
<14
Dan
Kraka
620000
640000
6180000
6160000
6140000
Northern Fault
Southern Fault A
Present-day pinchout of mobilised Zechstein
(b)
SF B
620000
640000
Northern Domain: Immobile Zechstein Salt (<100 ms TWT) or no Zechstein
Southern Domain: Mobile Zechstein Salt (~200 - 500 ms TWT)
Present-day seismic pinch-out of Potentially-Mobile Zechstein Salt
Study area for this work

Fig. 4

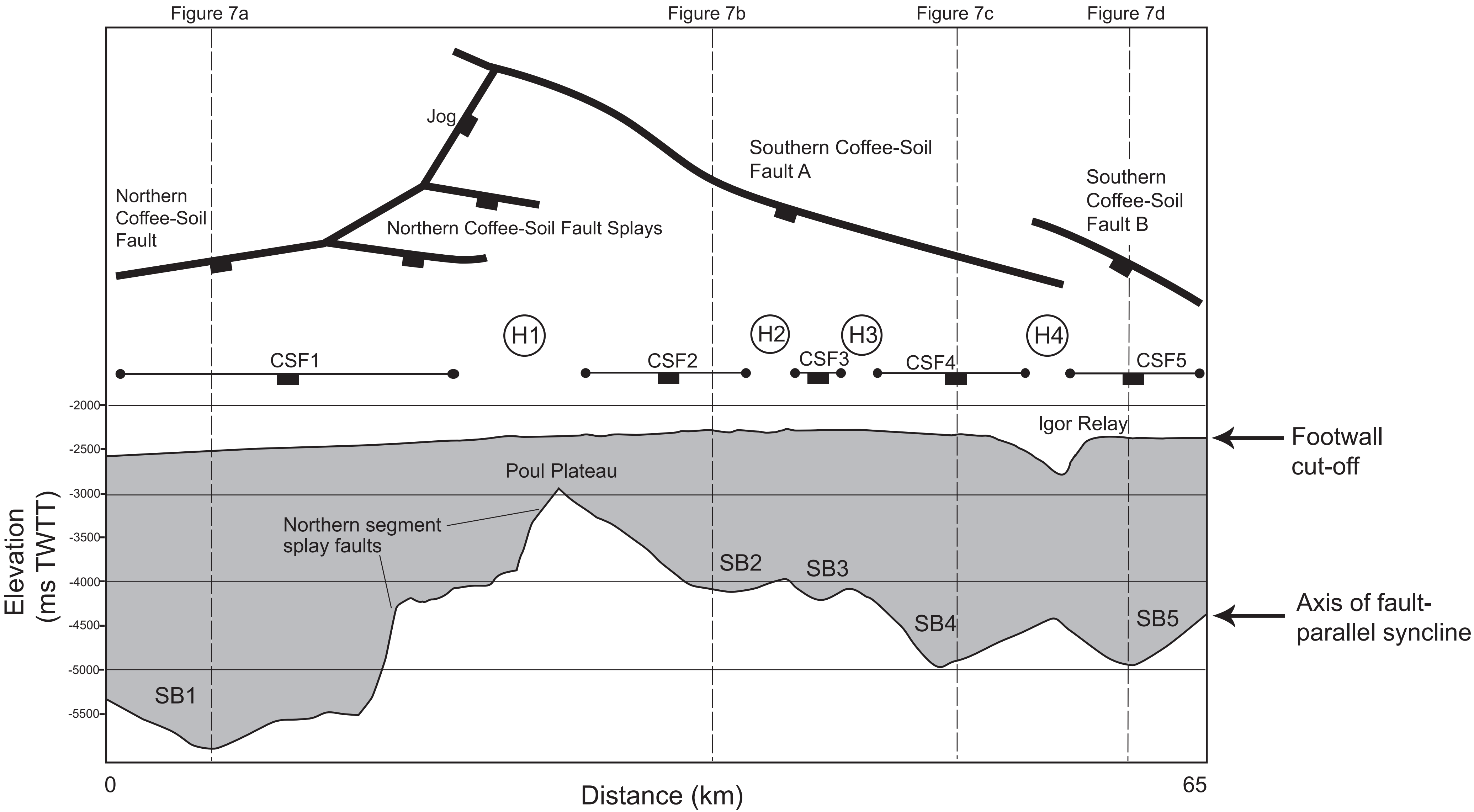

Figure 7a
Figure 7b
Figure 7c
Figure 7d
Jog
Southern Coffee-Soil Fault A
Southern Coffee-Soil Fault B
Northern Coffee-Soil Fault
Northern Coffee-Soil Fault Splays
H1
H2
H3
H4
CSF1
CSF2
CSF3
CSF4
CSF5
-2000
-2500
-3000
-3500
-4000
-4500
-5000
-5500
Igor Relay
Footwall cut-off
Poul Plateau
Northern segment splay faults
SB1
SB2
SB3
SB4
SB5
Axis of fault-parallel syncline
Elevation (ms TWTT)
0
65
Distance (km)

Fig. 5

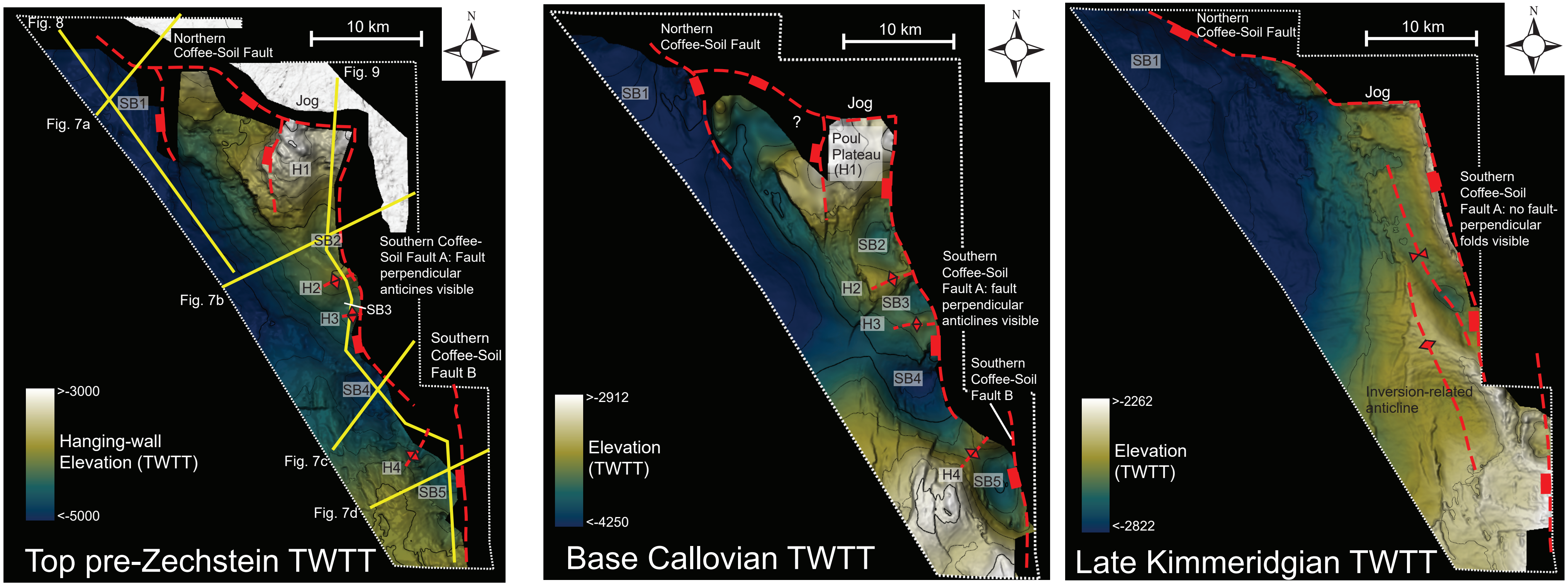

Fig. 8
Northern Coffee-Soil Fault
10 km
N
Fig. 9
Jog
SB1
Fig. 7a
H1
SB2
Southern Coffee-Soil Fault A: Fault perpendicular anticines visible
H2
SB3
Fig. 7b
H3
Southern Coffee-Soil Fault B
SB4
>-3000
Hanging-wall Elevation (TWTT)
<-5000
Fig. 7c
H4
SB5
Fig. 7d
Top pre-Zechstein TWTT
Northern Coffee-Soil Fault
10 km
N
SB1
?
Jog
Poul Plateau (H1)
SB2
H2
SB3
Southern Coffee-Soil Fault A: fault perpendicular anticlines visible
H3
SB4
Southern Coffee-Soil Fault B
>-2912
Elevation (TWTT)
<-4250
H4
SB5
Base Callovian TWTT
Northern Coffee-Soil Fault
10 km
N
SB1
Jog
Southern Coffee-Soil Fault A: no fault-perpendicular folds visible
Inversion-related anticline
>-2262
Elevation (TWTT)
<-2822
Late Kimmeridgian TWTT

Fig 6

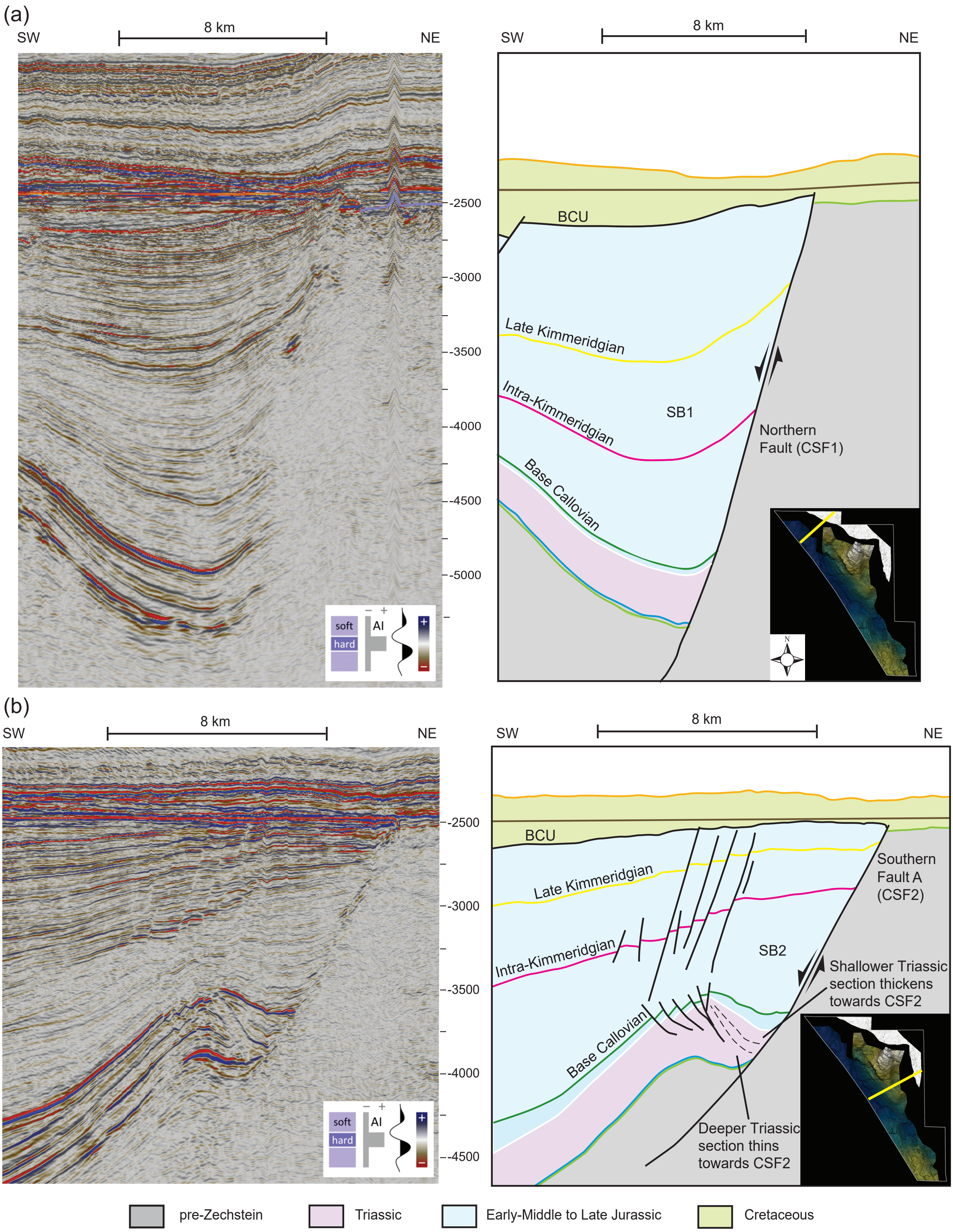

Fig 7 part 1 of 2

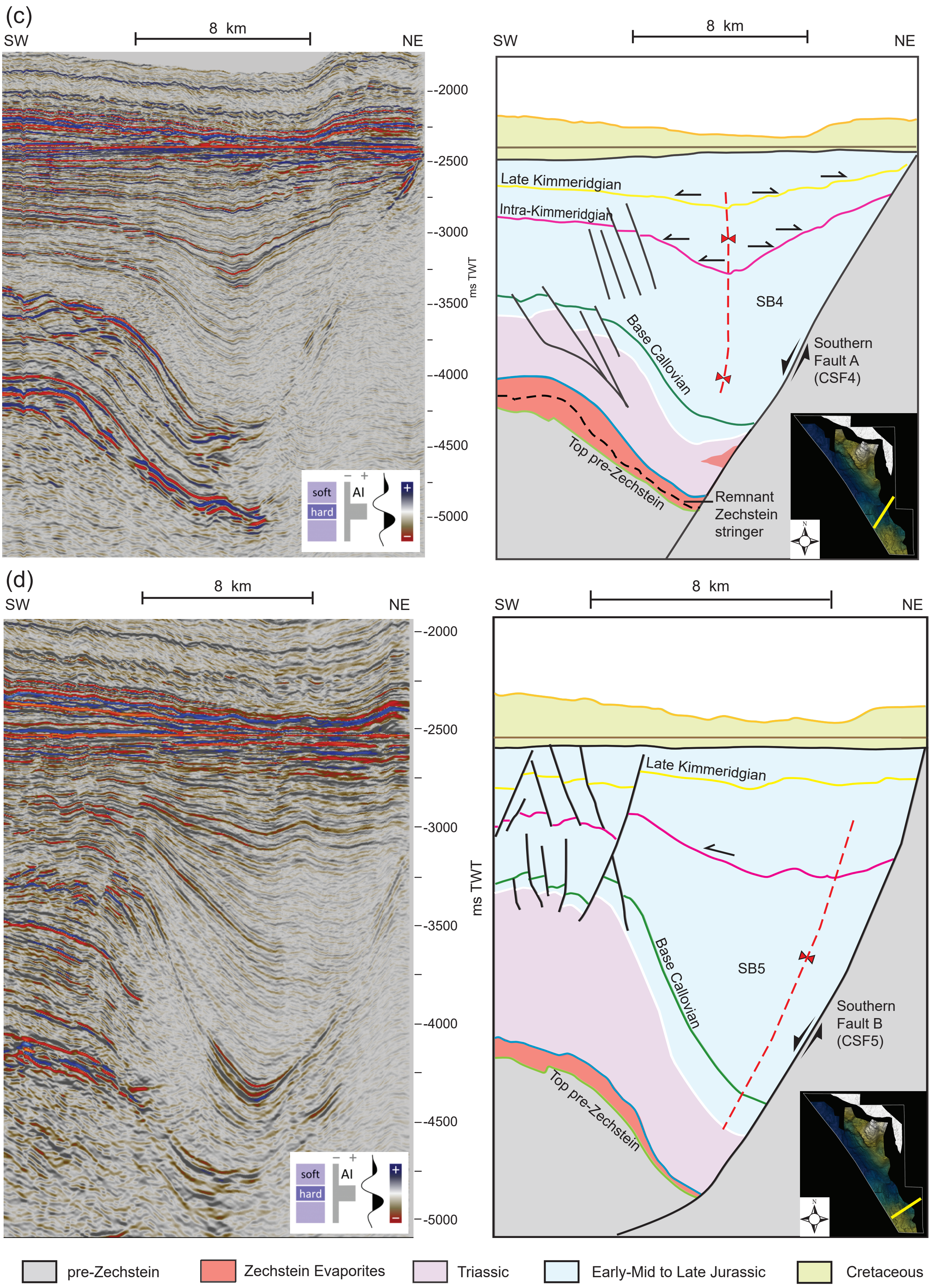

Fig 7 part 2 of 2

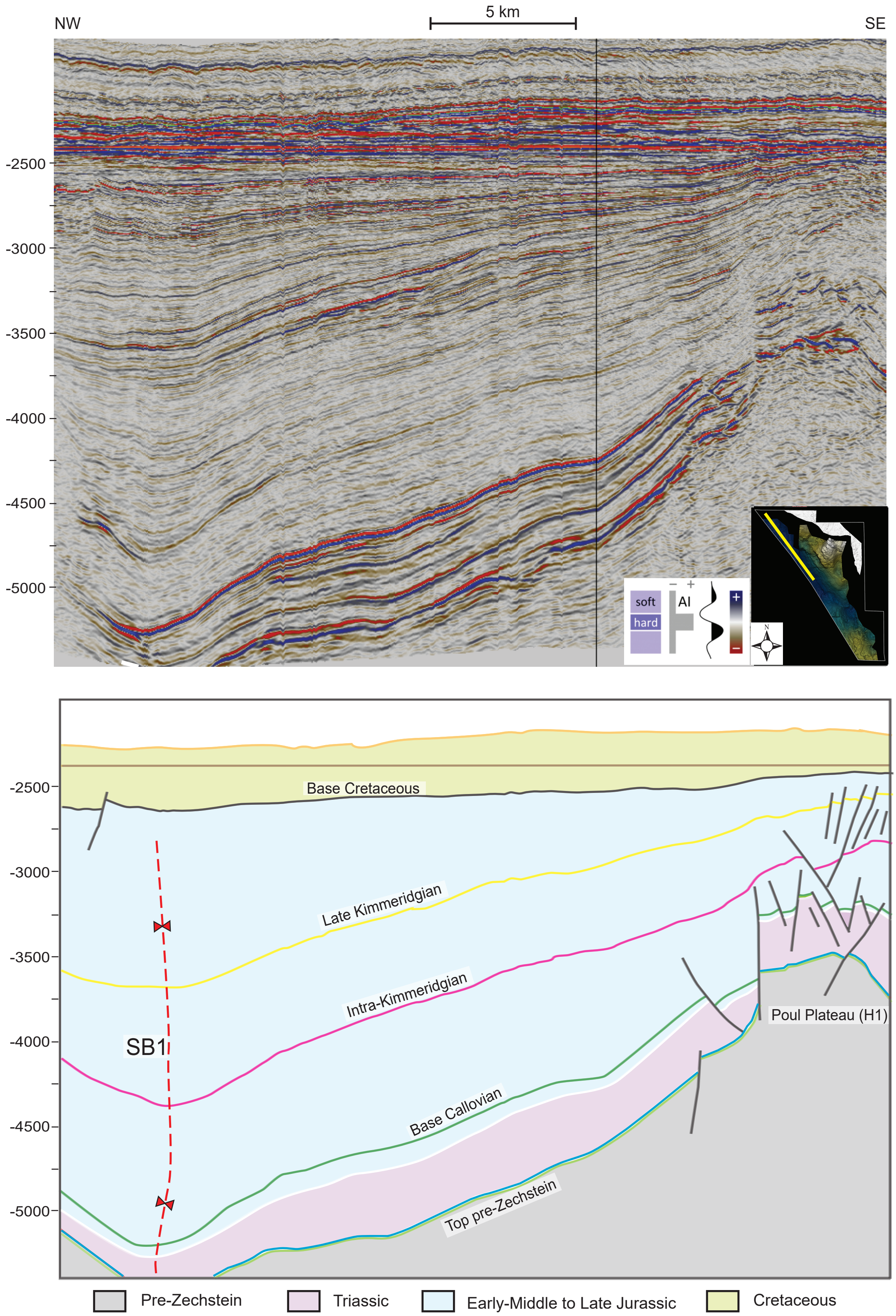
NW
5 km
SE
-2500
-3000
-3500
-4000
-4500
-5000
soft
hard
AI
Base Cretaceous
Late Kimmeridgian
Intra-Kimmeridgian
SB1
Base Callovian
Top pre-Zechstein
Poul Plateau (H1)
Pre-Zechstein
Triassic
Early-Middle to Late Jurassic
Cretaceous

Fig. 8

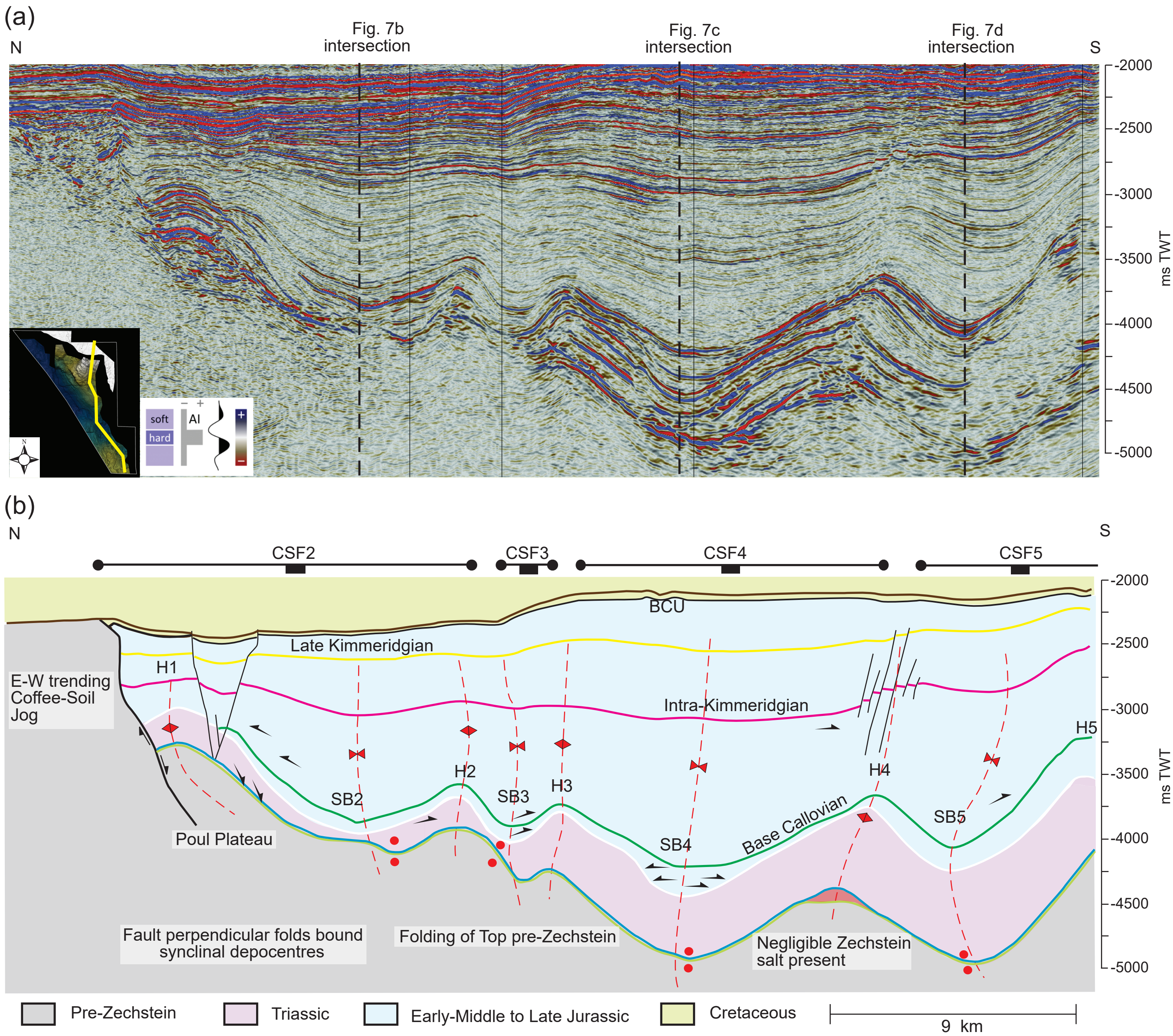

(a)
N
Fig. 7b intersection
Fig. 7c intersection
Fig. 7d intersection
S
-2000
-2500
-3000
-3500
-4000
-4500
-5000
ms TWT
soft
hard
AI
(b)
N
S
CSF2
CSF3
CSF4
CSF5
BCU
Late Kimmeridgian
H1
E-W trending Coffee-Soil Jog
Intra-Kimmeridgian
H5
H2
SB2
SB3
H3
H4
SB4
Base Callovian
SB5
Poul Plateau
Fault perpendicular folds bound synclinal depocentres
Folding of Top pre-Zechstein
Negligible Zechstein salt present
Pre-Zechstein
Triassic
Early-Middle to Late Jurassic
Cretaceous
9 km

Fig. 9

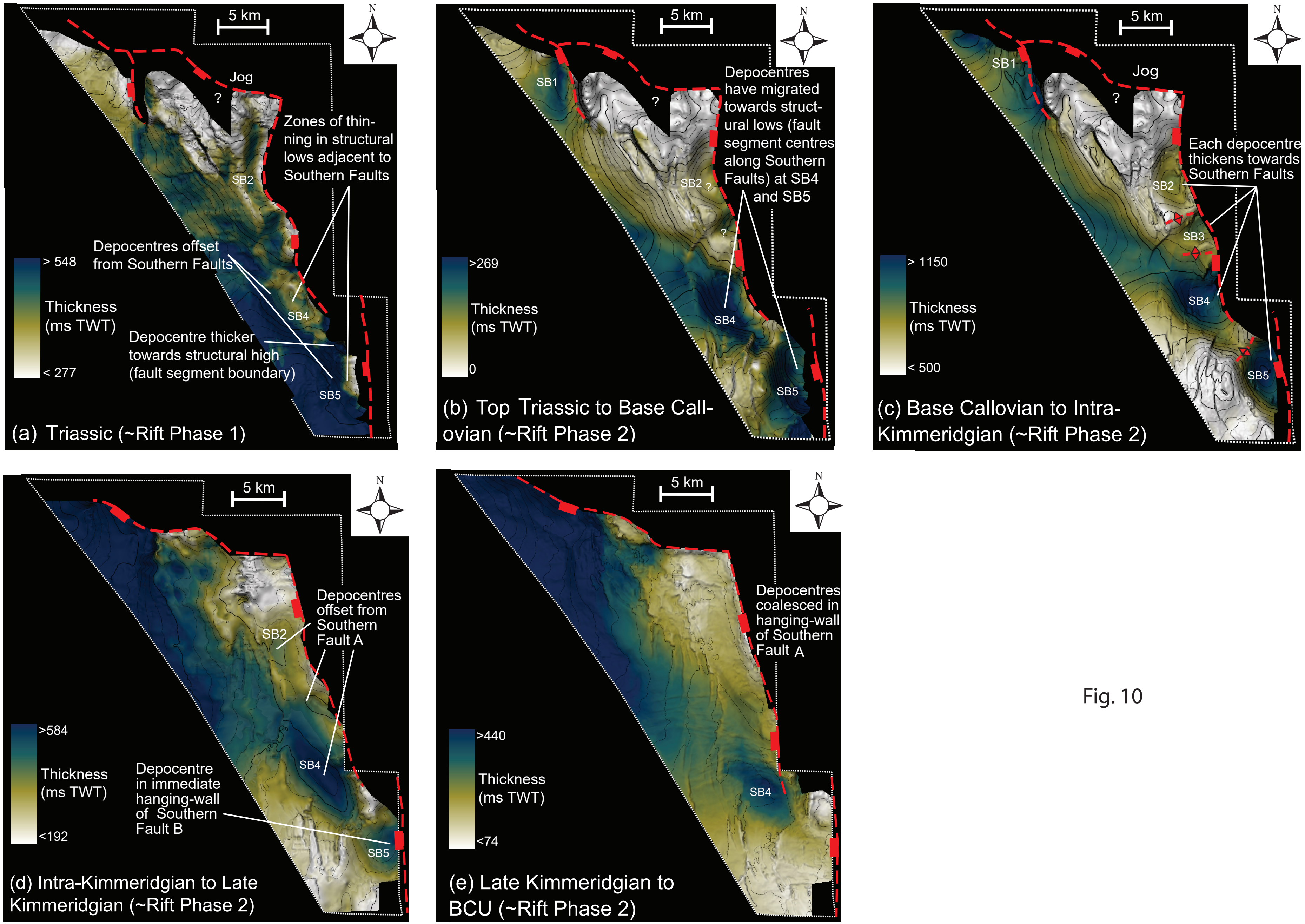
5 km
N
Jog
?
Zones of thin-ning in structural lows adjacent to Southern Faults
SB2
Depocentres offset from Southern Faults
SB4
Depocentre thicker towards structural high (fault segment boundary)
SB5
> 548
Thickness (ms TWT)
< 277
(a) Triassic (~Rift Phase 1)
5 km
N
SB1
?
Depocentres have migrated towards struct-ural lows (fault segment centres along Southern Faults) at SB4 and SB5
SB2 ?
?
SB4
SB5
>269
Thickness (ms TWT)
0
(b) Top Triassic to Base Call-ovian (~Rift Phase 2)
5 km
N
SB1
Jog
?
Each depocentre thickens towards Southern Faults
SB2
SB3
SB4
SB5
> 1150
Thickness (ms TWT)
< 500
(c) Base Callovian to Intra-Kimmeridgian (~Rift Phase 2)
5 km
N
Depocentres offset from Southern Fault A
SB2
SB4
Depocentre in immediate hanging-wall of Southern Fault B
SB5
>584
Thickness (ms TWT)
<192
(d) Intra-Kimmeridgian to Late Kimmeridgian (~Rift Phase 2)
5 km
N
Depocentres coalesced in hanging-wall of Southern Fault A
SB4
>440
Thickness (ms TWT)
<74
(e) Late Kimmeridgian to BCU (~Rift Phase 2)

Fig. 10

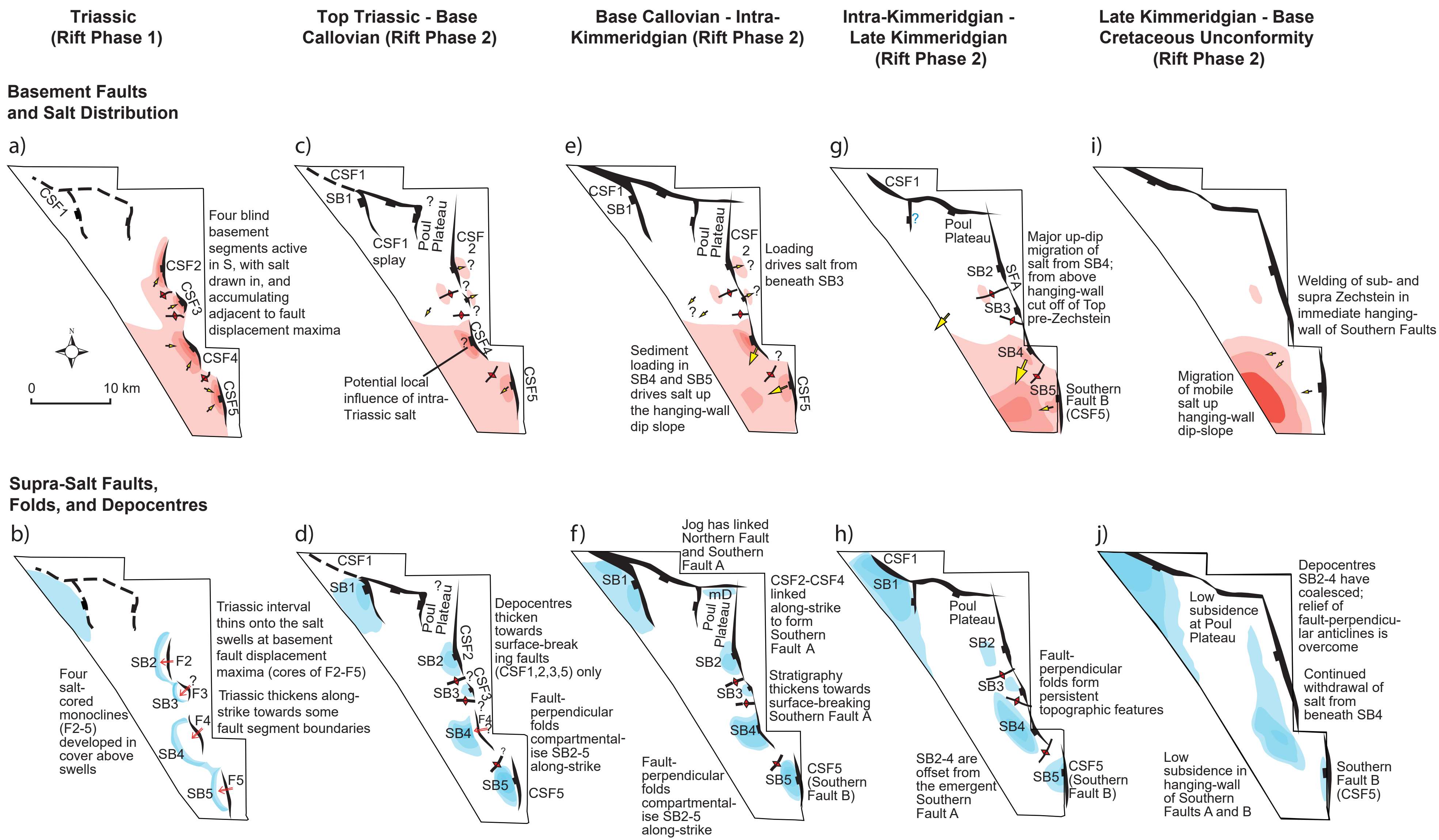
Triassic (Rift Phase 1)
Top Triassic - Base Callovian (Rift Phase 2)
Base Callovian - Intra-Kimmeridgian (Rift Phase 2)
Intra-Kimmeridgian - Late Kimmeridgian (Rift Phase 2)
Late Kimmeridgian - Base Cretaceous Unconformity (Rift Phase 2)
Basement Faults and Salt Distribution
a)
CSF1
CSF2
CSF3
CSF4
CSF5
Four blind basement segments active in S, with salt drawn in, and accumulating adjacent to fault displacement maxima
N
0
10 km
c)
CSF1
SB1
CSF1 splay
Poul Plateau
CSF 2
CSF4
CSF5
Potential local influence of intra-Triassic salt
e)
CSF1
SB1
Poul Plateau
CSF 2
CSF5
Loading drives salt from beneath SB3
Sediment loading in SB4 and SB5 drives salt up the hanging-wall dip slope
g)
CSF1
Poul Plateau
SB2
SFA
SB3
SB4
SB5
Major up-dip migration of salt from SB4; from above hanging-wall cut off of Top pre-Zechstein
Southern Fault B (CSF5)
i)
Welding of sub- and supra Zechstein in immediate hanging-wall of Southern Faults
Migration of mobile salt up hanging-wall dip-slope
Supra-Salt Faults, Folds, and Depocentres
b)
SB2
F2
SB3
F3
F4
SB4
SB5
F5
Four salt-cored monoclines (F2-5) developed in cover above swells
Triassic interval thins onto the salt swells at basement fault displacement maxima (cores of F2-F5)
Triassic thickens along-strike towards some fault segment boundaries
d)
CSF1
SB1
Poul Plateau
CSF2
SB2
SB3
CSF3
F4
SB4
SB5
CSF5
Depocentres thicken towards surface-breaking faults (CSF1,2,3,5) only
Fault-perpendicular folds compartmentalise SB2-5 along-strike
f)
Jog has linked Northern Fault and Southern Fault A
SB1
mD
Poul Plateau
SB2
SB3
SB4
SB5
CSF2-CSF4 linked along-strike to form Southern Fault A
Stratigraphy thickens towards surface-breaking Southern Fault A
CSF5 (Southern Fault B)
Fault-perpendicular folds compartmentalise SB2-5 along-strike
h)
CSF1
SB1
Poul Plateau
SB2
SB3
SB4
SB5
Fault-perpendicular folds form persistent topographic features
CSF5 (Southern Fault B)
SB2-4 are offset from the emergent Southern Fault A
j)
Low subsidence at Poul Plateau
Depocentres SB2-4 have coalesced; relief of fault-perpendicular anticlines is overcome
Continued withdrawal of salt from beneath SB4
Southern Fault B (CSF5)
Low subsidence in hanging-wall of Southern Faults A and B

Fig. 11

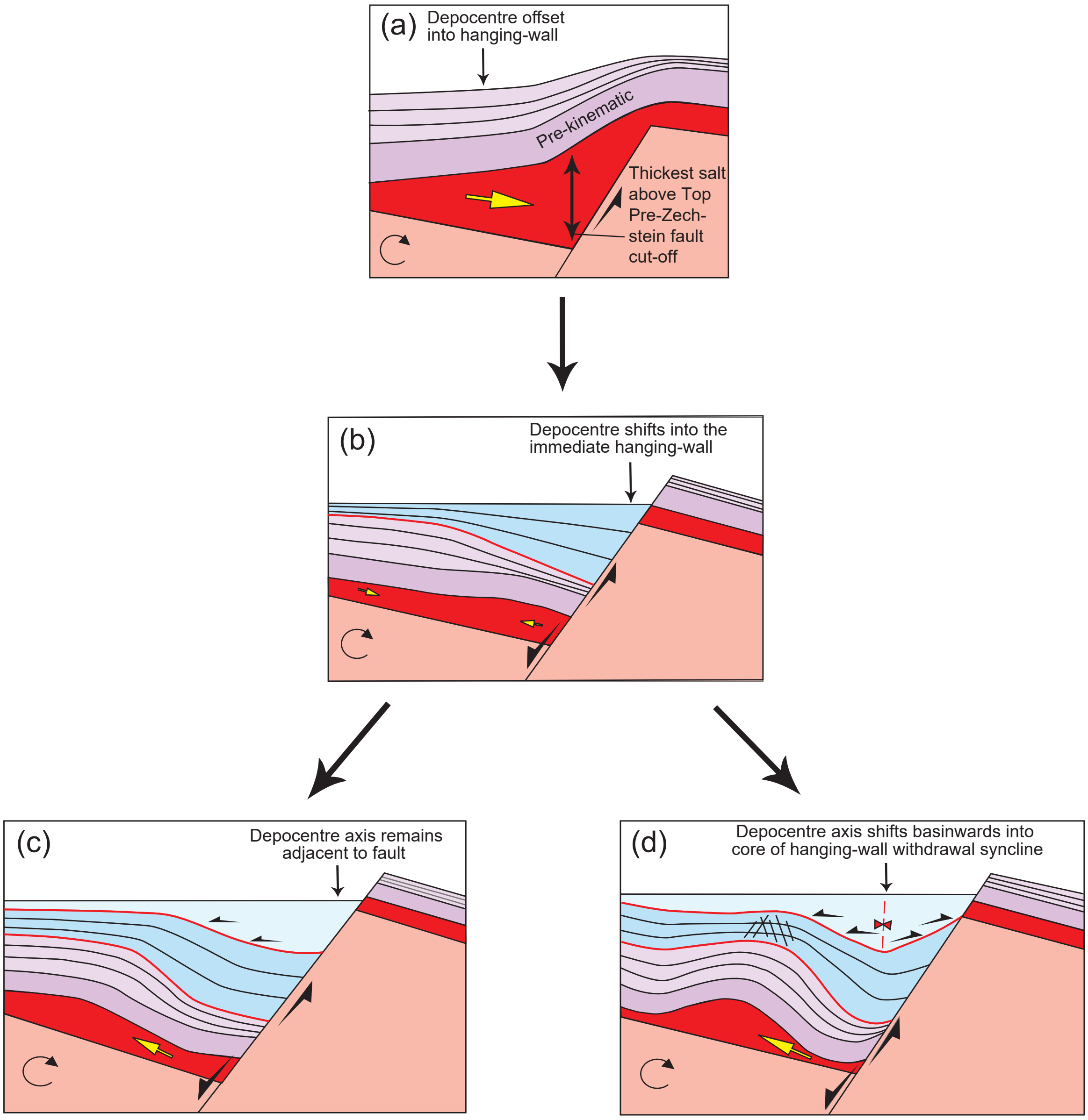
(a) Depocentre offset into hanging-wall
Pre-kinematic
Thickest salt above Top Pre-Zech-stein fault cut-off
(b)
Depocentre shifts into the immediate hanging-wall
(c)
Depocentre axis remains adjacent to fault
(d)
Depocentre axis shifts basinwards into core of hanging-wall withdrawal syncline

Fig. 12

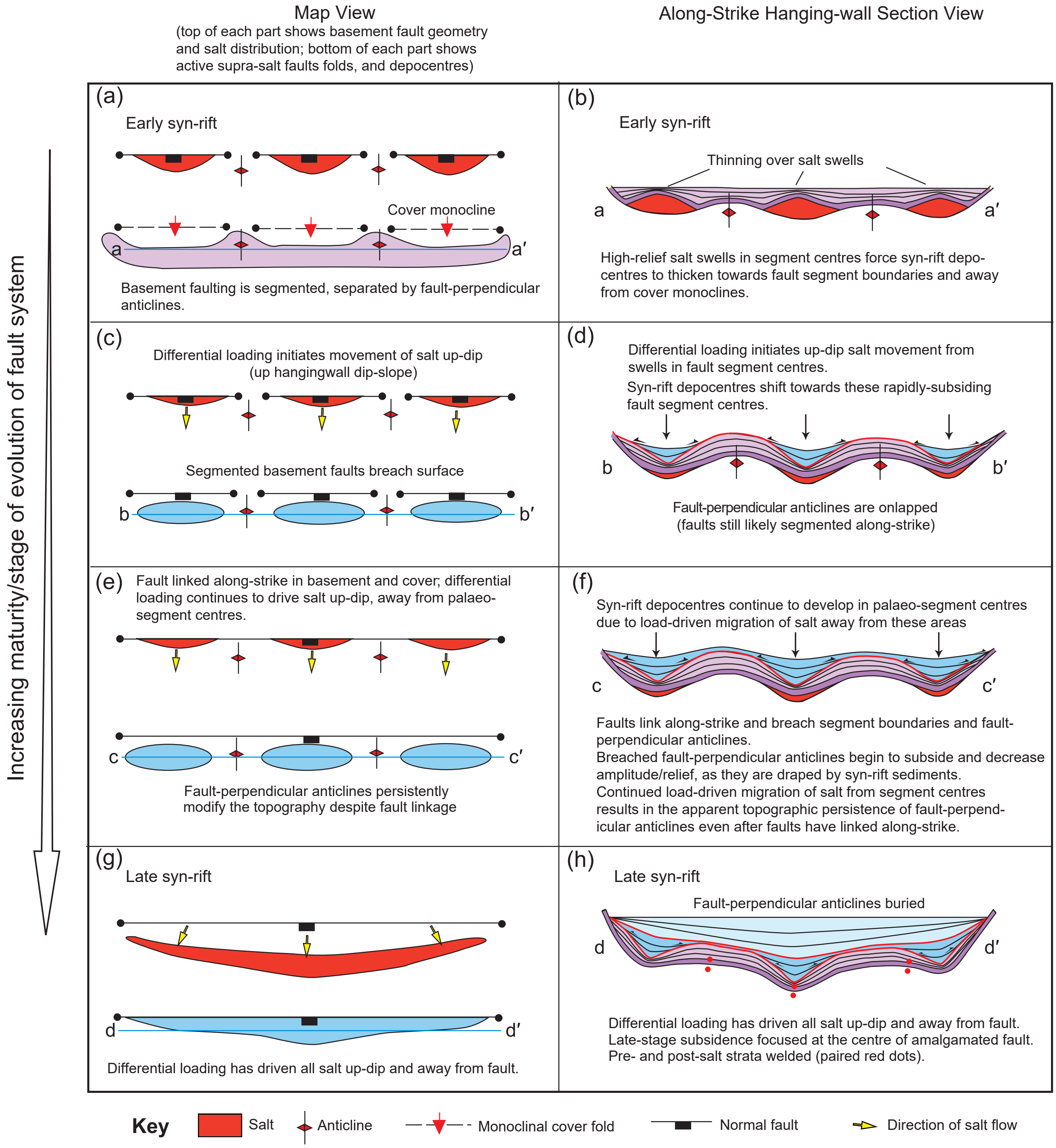
Map View
(top of each part shows basement fault geometry and salt distribution; bottom of each part shows active supra-salt faults folds, and depocentres)
Along-Strike Hanging-wall Section View
Increasing maturity/stage of evolution of fault system
(a)
Early syn-rift
Cover monocline
a
a′
Basement faulting is segmented, separated by fault-perpendicular anticlines.
(b)
Early syn-rift
Thinning over salt swells
a
a′
High-relief salt swells in segment centres force syn-rift depocentres to thicken towards fault segment boundaries and away from cover monoclines.
(c)
Differential loading initiates movement of salt up-dip (up hangingwall dip-slope)
Segmented basement faults breach surface
b
b′
(d)
Differential loading initiates up-dip salt movement from swells in fault segment centres.
Syn-rift depocentres shift towards these rapidly-subsiding fault segment centres.
b
b′
Fault-perpendicular anticlines are onlapped (faults still likely segmented along-strike)
(e)
Fault linked along-strike in basement and cover; differential loading continues to drive salt up-dip, away from palaeo-segment centres.
c
c′
Fault-perpendicular anticlines persistently modify the topography despite fault linkage
(f)
Syn-rift depocentres continue to develop in palaeo-segment centres due to load-driven migration of salt away from these areas
c
c′
Faults link along-strike and breach segment boundaries and fault-perpendicular anticlines.
Breached fault-perpendicular anticlines begin to subside and decrease amplitude/relief, as they are draped by syn-rift sediments.
Continued load-driven migration of salt from segment centres results in the apparent topographic persistence of fault-perpendicular anticlines even after faults have linked along-strike.
(g)
Late syn-rift
d
d′
Differential loading has driven all salt up-dip and away from fault.
(h)
Late syn-rift
Fault-perpendicular anticlines buried
d
d′
Differential loading has driven all salt up-dip and away from fault.
Late-stage subsidence focused at the centre of amalgamated fault.
Pre- and post-salt strata welded (paired red dots).
Key
Salt
Anticline
Monoclinal cover fold
Normal fault
Direction of salt flow

Fig. 13